

# Radar Depth Sounder Processing and Digital Thickness Map of Outlet Glaciers

By

Harish N. Ramamoorthy

Bachelor of Engineering, Instrumentation and Control,  
University of Madras,  
Chennai, India, 2001

Submitted to the Department of Electrical Engineering and Computer Science and the  
Faculty of the Graduate School of the University of Kansas in partial fulfillment of  
the requirements for the degree of Master of Science

---

Dr. Pannirselvam Kanagaratnam, Chair

---

Dr. Prasad Gogineni

---

Dr. David Braaten

Date of Defense: May 17<sup>th</sup>, 2004

## **Abstract**

In the advent of global warming's threatening effects on the environment, quantifying it by monitoring the mass balance of the ice sheets has become one of the major challenges in the field of remote sensing. The rate at which polar ice sheets melt is attributed to global warming. Ice sheet thickness is intrinsically related to the flow dynamics of outlet glaciers that drain a major portion of the polar ice into the ocean. To understand the mechanism of glacial flow, knowledge of the topography of the bedrock is essential.

Since 1993, when NASA initiated a program to measure the mass balance of the ice sheets, the Radar Systems and Remote Sensing Laboratory (RSL) at the University of Kansas has been conducting experiments in Greenland and Antarctica using radar depth sounder systems to measure the thickness of the polar ice sheets. Radar returns are collected over these regions and are then processed to interpret the echo from the surface and bedrock to determine the ice thickness.

In this project, we investigate the signal-processing techniques applied to the radar return to enhance the signal-to-noise ratio and accurately determine ice thickness. The thickness data collected over the three main outlet glaciers of Jakobshavns Isbrae, Petermann and Kangerlussuaq are developed into digital ice thickness maps by

interpolating the measured data into a continuous surface. Three-dimensional maps of the bed terrain help in understanding the glacial flow mechanism.

## **Acknowledgements**

I would like to express my sincere gratitude to my project supervisor Dr.Pannirselvam Kanagaratnam for guiding me throughout my work at the Radar Systems and Remote Sensing Laboratory. I would like to thank my advisor Dr.Prasad Gogineni for giving me an opportunity to work on this project, for his guidance and for serving on my defense committee. I thank Dr. David Braaten for his valuable suggestions and for accepting to serve on my committee.

I would like to specially acknowledge John Kostelnick, Department of Geography, PRISM Outreach, for being ever ready to answer my numerous questions on arcGIS amidst his busy schedule. It gives me immense pleasure to acknowledge the wonderful association I have had with the members of the RSL team. This association has helped me become a better team player. My sincere thanks to Ms.Kelly Mason, Program Assistant, for editing this document.

I would like to thank my parents and sister for supporting me with their love, encouragement and motivation at every stage of my life. My special token of love to my late grandparents without whose blessings I wouldn't have come this far in my life.

I thank all my friends at KU for the great time that I spent with them that will remain green forever. I would like to thank my friend Vivek Ramachandran for all his support and encouragement through thick and thin.

As ever, I owe all the credits for whatever I have achieved to the Almighty.

*Dedicated*  
*To My*  
*Wonderful Family*

# Contents

<b>1</b>	<b>INTRODUCTION.....</b>	<b>1</b>
1.1	Significance of Remote Sensing of Glacial Ice.....	1
1.2	Role of Outlet Glaciers in Sea-Level Rise.....	2
1.3	History of Radar Depth Sounders at KU.....	2
1.4	Objectives of this Project.....	3
1.5	Organization.....	4
<b>2</b>	<b>DESCRIPTION OF RADAR DEPTH SOUNDER.....</b>	<b>5</b>
2.1	Chirp Radar.....	5
2.2	System Description.....	7
2.2.1	Improved Coherent Antarctic and Arctic Radar Depth Sounder.....	7
2.2.2	Advanced COherent Radar Depth Sounder.....	8
2.2.3	Advantages of ACORDS over ICARDS.....	11
<b>3</b>	<b>EXPERIMENT DESCRIPTION AND SIGNAL PROCESSING.....</b>	<b>12</b>

<b>3.1</b>	<b>Measurements over Antarctica.....</b>	<b>12</b>
3.1.1	Operation of Radar.....	14
3.1.2	ICARDS Data File Structure .....	15
<b>3.2</b>	<b>Measurements over Greenland.....</b>	<b>19</b>
3.2.1	ACORDS Data File Structure.....	20
<b>3.3</b>	<b>Signal Processing.....</b>	<b>24</b>
3.3.1	Pulse Integration: Software.....	24
3.3.2	D.C.Offset Removal.....	25
3.3.3	Gain Compensation.....	26
3.3.4	Coherent Noise Reduction .....	30
3.3.5	Multiple-Echo Cancellation .....	32
3.3.6	Inter Gain Compensation .....	35
<b>4</b>	<b>DATA INTERPOLATION .....</b>	<b>37</b>
<b>4.1</b>	<b>Interpolating the Thickness Data .....</b>	<b>37</b>
4.1.1	Types of Interpolation.....	38
4.1.2	Kriging Interpolation .....	39
4.1.3	Kriging – Procedure.....	40
<b>4.2</b>	<b>Tool Used .....</b>	<b>45</b>
<b>5</b>	<b>IMPLEMENTATION AND RESULTS.....</b>	<b>47</b>

<b>5.1</b>	<b>Kangerlussuaq Glacier .....</b>	<b>47</b>
5.1.1	Interpolation to Raster Thickness Data.....	50
<b>5.2</b>	<b>Jakobshavn Isbrae .....</b>	<b>54</b>
5.2.1	Description of the Jakobshavn Dataset.....	57
5.2.2	Interpolation to Raster Thickness Data.....	61
<b>5.3</b>	<b>Petermann Glacier .....</b>	<b>68</b>
5.3.1	Interpolation to Raster Thickness Data.....	71
<b>6</b>	<b>CONCLUSION AND FUTURE WORK.....</b>	<b>78</b>
<b>6.1</b>	<b>Conclusion .....</b>	<b>78</b>
<b>6.2</b>	<b>Pointers to Future Work .....</b>	<b>79</b>

## List of Figures

2.1	Functional Block Diagram of ACORDS.....	9
3.1	Flightlines of the Antarctic Mission, November – December 2002 .....	12
3.2	Radio echogram and Thickness Profile along Pine Island Glacier .....	19
3.3	Flightlines of the Greenland Mission, May 2003 .....	20
3.4	Radio Echogram and Thickness profile of ice sheet sounded near Petermann Glacier .....	24
3.5	Result of Pulse Integration .....	26
3.6	Radar Echogram of the Pine Island Glacier Illustrating the effect of gain compensation .....	30
3.7	Return Signal measured by ACORDS near Humboldt Glacier: Result of Coherent Noise Reduction .....	32
3.8	Noise Spectrum in the High Gain Channel .....	33
3.9 a	Echogram illustrating Multiple Echo .....	34
3.9 b	Multiple-echo has been eliminated making the interpretation of the echo from the bedrock easier .....	36
4.1	Interpolation of Discontinuous Samples into Raster .....	39
4.2	A Semivariogram .....	42
4.3	Semivariogram of Data over Jakobshavn .....	43
5.1 a	Flightlines over Kangerlussuaq .....	49
5.1 b	Kangerlussuaq Flightlines on a High Resolution Image of the Glacier and thickness profiles of major flight paths .....	50

5.2 a	3D View of the Interpolated Data over Kangerlussuaq .....	53
5.2 b	3D View of the Interpolated Data over Kangerlussuaq on a Wider Color Spectrum .....	54
5.3 a	Flightlines over Jakobshavn Isbrae .....	55
	(Missing data across the Channel is shown)	
5.3 b	Jakobshavn Flightlines on a High Resolution Image of the Glacier and thickness profiles of some flight paths across the channel .....	57
5.4	Data Description and Data Filtering over Jakobshavn .....	60
5.5	Echogram Illustrating the Channel in Jakobshavn and the Thickness Profile Across the Channel .....	62
5.6	Interpolated Bed Topography of Jakobshavn (above); View of the Interpolated Channel (below) .....	66
5.7 a	3D View of the Interpolated Data over Jakobshavn on a Wider Color Spectrum .....	67
5.8 b	3D View of the Interpolated Data over Jakobshavn Channel on a Wider Color Spectrum .....	68
5.8 a	Flightlines over Petermann Glacier .....	69
5.8 b	Petermann Flightlines on a High Resolution Image of the Glacier and Thickness Profiles of crossovers .....	71
5.9	Interpolated Bed Topography of Petermann (above); Crossover Region (below) .....	74
5.9 a	3D View of the Interpolated Data over Petermann on a Wider Color Spectrum .....	75
5.10 b	3D View of the Interpolated Data over Crossover Region on a Wider Color Spectrum .....	76
5.11	Echogram and Thickness Plot of Petermann Up the Channel Towards the Grounding Line .....	77

## List of Tables

2.1	System Parameters of ICARDS .....	8
2.2	System Parameters of ACORDS .....	11
3.1	ICARDS Data Header Format .....	16
3.2	Radar Setting of ICARDS .....	17
3.3	ICARDS Data Format .....	18
3.4	ICARDS Datatypes .....	18
3.5	ACORDS Datatypes .....	21
3.6	Radar Setting of ACORDS .....	22
3.7	ACORDS Data Format .....	23

# 1 Introduction

---

## 1.1 Significance of Remote Sensing of Glacial Ice

Polar ice sheets in Greenland and Antarctica contain about 90% of the world's fresh water. The Greenland ice sheet has been melting for about 15,000 years and has retreated to its present size [1]. As a result of the melting of the polar ice sheets, sea level has been rising at an alarming rate of 2 mm/year over the past century. This is attributed to global warming, and according to a report in *Nature* [2], if global warming continues at its present rate; the rest of Greenland's ice sheet would melt in a thousand years. If the Greenland ice sheet were to melt completely, it would cause the sea level to rise about 7 m, with devastating consequences to coastal regions. Monitoring the mass balance of the ice sheet will help scientists understand the effects of the global warming on ice sheets and help to quantify their contribution to sea level rise. Ice thickness is an important parameter in computing the mass balance of glacial ice. Net ice sheet mass balance and glacier flow characteristics are intrinsically related to the thickness of the ice sheet. Glacier dynamics can be modeled using ice thickness, and its measure is a very critical and sensitive boundary condition, such that even small errors in ice thickness data can result in large errors in the predicted ice sheet behavior.

## **1.2 Role of Outlet Glaciers in Sea-Level Rise**

Ice bodies that play a very important role in the rapid draining of inland ice sheets are outlet glaciers. An outlet glacier is a valley glacier, which drains an inland ice sheet or ice cap and flows through a gap in the peripheral mountains. They move from accumulation areas through mountainous terrain to the sea. Outlet glaciers also include broad, well-defined lobes of glacier ice that protrude from an ice cap or inland ice sheet and spread over areas of low relief [3].

It is very important to understand the flow mechanism of the outlet glaciers. Accurate knowledge of ice thickness data is required to characterize the flow mechanism of the outlet glaciers. However, radio echo sounding of outlet glaciers is difficult because of high signal absorption due to warm ice, signal clutter caused by rough, crevassed ice surfaces, and reflections from nearby valley sides.

## **1.3 History of Radar Depth Sounders at KU**

In an attempt to obtain accurate ice thickness measurements, the Radar Systems and Remote Sensing Laboratory (RSL) at the University of Kansas has been making measurements over the Greenland ice sheet every year since 1993 on a NASA P-3 aircraft equipped with a radar depth sounder. Improvements have been made to the radar each year to overcome limitations faced in the previous year.

The RSL team used the Coherent Antarctic Radar Depth Sounder (CARDS) from 1989 to 1995, and the Improved Coherent Antarctic Radar Depth Sounder (ICARDS) [4] was used in 1996. Some of the limitations of ICARDS were overcome by the compact Next Generation Coherent Radar Depth Sounder (NGCORDS), which was flown from 1997 till 2002. These radars were not very successful in obtaining good thickness measurements at the outlet glaciers, and this led to the development of the Advanced COherent Radar Depth Sounder (ACORDS), which was used to sound the outlet glaciers in Greenland in the field experiment in the summer of 2003.

#### **1.4 Objectives of this Project**

This project has a two-fold objective. The first is to detail the signal processing aspects of determining the thickness of glacial ice. The second is to produce a thickness profile of the outlet glaciers in Greenland. In November and December, 2002 we made airborne ice thickness measurements for the first time over the Antarctic ice sheet with ICARDS. ACORDS was used for the first time in 2003 to measure the thickness of the Greenland ice sheet. The data processing techniques to extract thickness information from the measurements taken by these two radars will be described in detail in this project.

The three outlet glaciers in Greenland, Jakobshavn Isbrae, Petermann and Kangerlussuaq drain a large amount of Greenland ice sheet into the ocean. The

thickness, bottom and the surface topographies have been determined from the data from ACORDS. The thickness data available from these regions over the past seven years have been used to develop a three-dimensional thickness map of the bed, which gives more information about the bed terrain. At regions in Jakobshavn glacier, the airborne depth sounder was unable to measure the thickness of the ice sheet because of heavy scattering of the transmitted signals by deep crevasses. In these regions, thickness data have been included from seismic measurements.

## **1.5 Organization**

This report has been organized into six chapters. The second chapter describes the radar depth sounder systems that were used in the field experiments in Antarctica in December 2002 and Greenland in May 2003. The third chapter describes the signal processing aspects of thickness measurement. The image processing aspects of Interpolating the data and visualizing the data from the three outlet glaciers are explained in the fourth chapter. The images and their analysis are presented in the fifth chapter. The concluding chapter gives a brief summary of the report and pointers for future work.

## 2 Description of Radar Depth Sounder

---

This chapter describes the concept of pulse compression and the basic principles underlying the operation of the depth sounder. The first half explains the Improved Coherent Antarctic and Arctic Radar Depth Sounder (ICARDS) that was used in the Antarctic field experiments and the later half deals with the Advanced COherent Radar Depth Sounder (ACORDS) used in the Greenland field experiments.

### 2.1 Chirp Radar

The range resolution of radar in a particular medium is given by

$$R = \frac{c}{2B}$$

where  $R$  is the range resolution,  $c$  is the velocity of propagation of EM waves in the medium and  $B$  is the bandwidth of the transmit signal.

The energy contained in a pulse is given by

$$E = P \times \tau$$

where  $E$  is the energy contained in a pulse and  $P$  is the peak transmit power.

High peak power is required for long detection range and the transmit pulse needs to be extremely narrow for fine range resolution. Since the upper level of the peak

power that can be transmitted is practically limited by the hardware, high power levels can be achieved by transmitting wider pulses. A wider pulse will result in a poor resolution. A solution to achieving high power and good range resolution is *Pulse compression*.

Linear frequency modulation or chirp is a pulse compression technique in which the frequency of each transmitted pulse is increased or decreased at a constant rate throughout its transmission duration. Hence, the received pulses will have a linear increase or decrease in frequency. On passing the received pulses through a *matched* filter that introduces a time lag inversely proportional to frequency, the resulting pulses are compressed. Radars that employ the pulse compression technique to achieve long detection range and fine resolution are called *pulse-compressed radars*.

In pulse-compressed radars, a long frequency modulated pulse is transmitted. At the receiver end the return pulse is compressed to a width  $1/B$ . The ratio of the transmitted pulse width  $T$  to the compressed pulse width  $\tau$  gives the pulse compression ratio. Pulse compression is the basis of operation of the radar depth sounder systems.

## 2.2 System Description

### 2.2.1 Improved Coherent Antarctic and Arctic Radar Depth

#### Sounder

The Improved Coherent Antarctic and Arctic Radar Depth Sounder (ICARDS) built by Chuah [5] was used in experiments over the Patagonian glaciers in Chile and the Pine Island and Thwaites glacier in Antarctica in the Austral summer of 2002. ICARDS transmits a chirp signal with peak power of 200 W centered at 150 MHz for pulse duration of 1.6  $\mu$ s. The transmit signal is sent through the transmit antenna and the backscattered echoes are coupled to the receiver section through the receive antenna. These echoes are amplified, compressed and demodulated into two channels, namely, In-phase channel (I – channel) and Quadrature channel (Q – channel). Surface Acoustic Wave devices are used for generating the transmit pulse and to perform pulse compression. The return signals from the I and Q channels are then digitized by two 12-bit A/D converters at a rate of 18.75 megasamples per second. Data from 256 consecutive transmit-receive periods are coherently integrated by summing the complex data vectors from the I and Q channels. Integration or averaging reduces noise and decreases the data rate, thus enabling ease of storage. A selectable PRF and a 37.5 MHz clock signal synchronize the operation of the entire radar system. Two 4–element  $\lambda/2$  dipole arrays act as transmit and receive antennas. Description of the system parameters of ICARDS is given in Table (2.1).

<b>Description of Radar Parameter</b>	<b>Characteristic/Value</b>	<b>Units</b>
Radar Type	Pulse Compression	–
RF Carrier Frequency	150	MHz
RF Up-Chirp Bandwidth	17.00	MHz
Transmitted Pulse Width	1.6	$\mu$ s
Compressed Pulse Width	60	ns
Peak Transmit Power	200	W
PRF	Selectable	KHz
Number of Coherent Integrations	0 – 64,000	–
Number of Incoherent Integrations	0 – 64,000	–
A/D dynamic range	12 – bit, 72	dB
Receiver Dynamic Range	>110	DB
Sampling Period	53.3	ns
Range Resolution	4.494	m
Antenna	4 – element $\lambda/2$ dipole array	–

Table 2.1: System Parameters of ICARDS

### 2.2.2 Advanced COherent Radar Depth Sounder

The radar depth sounder used in the 2003 field experiments in Greenland is a modified and improved version of the ICARDS. This version, named the Advanced COherent Radar Depth Sounder (ACORDS) [6] operates at a center frequency of 150MHz. A functional block diagram of ACORDS is given in Figure (2.1). A selectable PRF signal triggers the chirp pulse generated by a waveform generator and is amplified to 200 W before transmission.

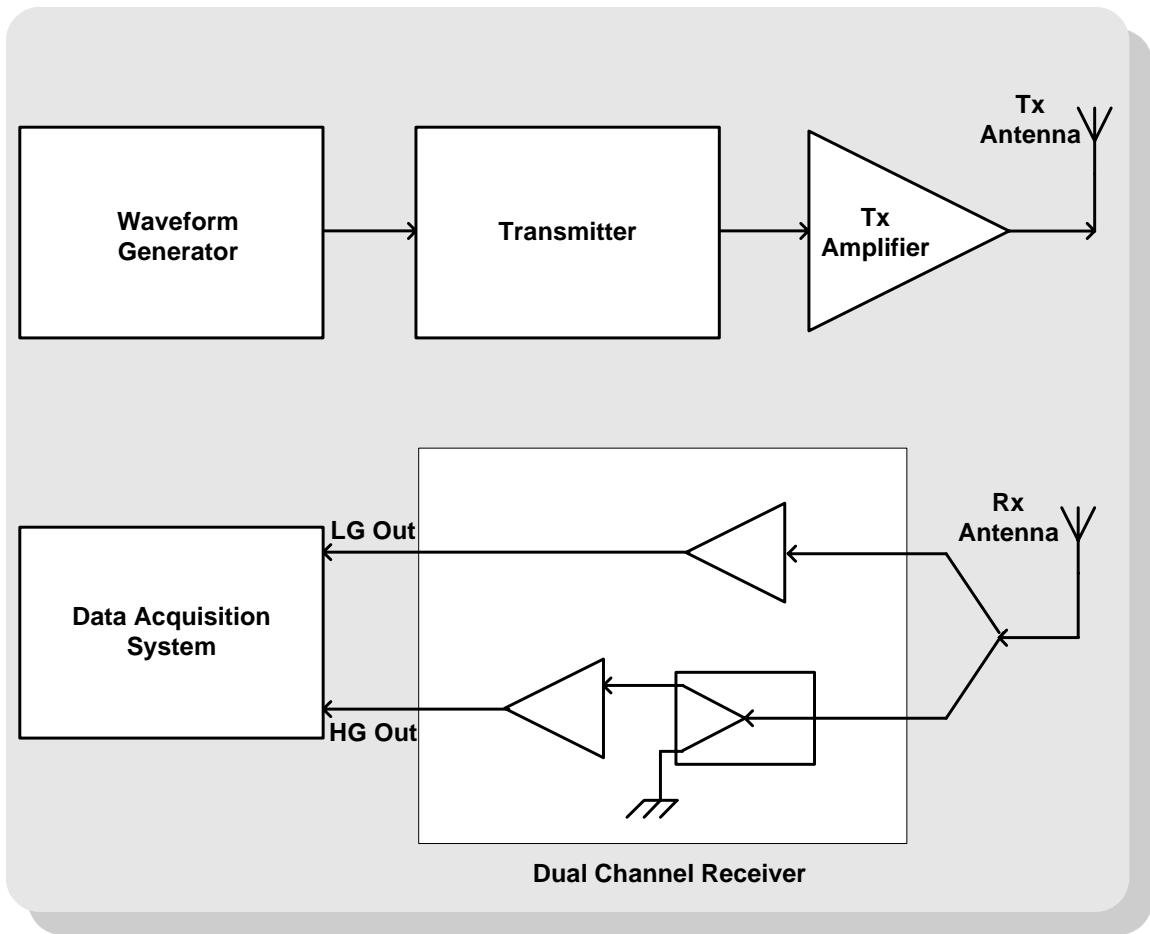


Figure 2.1: Functional Block Diagram of ACORDS

The chirp pulse is frequency modulated over a bandwidth of 17MHz with pulse duration selectable between 200 ns and 10  $\mu$ s. The 17 MHz bandwidth gives it a range resolution of 4.494 m. A receiver-blanking switch prevents the leakage signal from damaging the receiver during the transmission events. The received backscattered echoes are amplified by the receiver and split into two RF channels, namely, the Low Gain (LG) channel and the High Gain (HG) channel. The gain in both the channels can be selected by controlling the digital attenuation. The stronger

returns from the air/ice interface and some internal layers are recorded in the LG channel and the weaker returns are recorded in the HG channel. A high gain blanking switch prevents the stronger returns from saturating the HG channel amplifier. The received echoes from the HG and LG channels are digitized at a rate of 55 megasamples/s in the data acquisition system using a 12-bit A/D converter. The digitized data are stored in the host computer after integrating the LG and HG channel returns from the receiver. A four element  $\lambda/2$  dipole antenna arrays act as the transmit and receive antennas. Description of the system parameters of ACORDS is given in Table (2.2).

<b>Description of Radar Parameter</b>	<b>Characteristic/Value</b>	<b>Units</b>
Radar Type	Pulse Compression	–
RF Carrier Frequency	150	MHz
RF Up-Chirp Bandwidth	17.00	MHz
Transmitted Pulse Width	Selectable (200ns – 10 $\mu$ s)	$\mu$ s
Range Sidelobes	<36	dB
Peak Transmit Power	200	W
PRF	Selectable	KHz
Number of Coherent Integrations	32 – 1024	–
Number of Incoherent Integrations	0 – 64,000	–
A/D dynamic range	12 – bit, 72	dB
Receiver Dynamic Range	>110	DB
Sampling Period	18.182	ns
Range Resolution	4.494	m
Antenna	4 – element $\lambda/2$ dipole array	–

Table 2.2: System Parameters of ACORDS

### **2.2.3 Advantages of ACORDS over ICARDS**

ACORDS was used for the field experiment in Greenland in summer 2003. Some of the improvements of ACORDS over ICARDS are listed below.

- In ICARDS, the pulse compression using a matched filter approach produced large range sidelobes at the output of the filter and these sidelobes were masking the weaker returns from the bedrock and some deeper layers. This was overcome by digitally generating the pulse and using a digital mismatched filter to compress the pulse.
- In ACORDS, since the transmit waveform is digitally generated, we can produce waveforms that take into account the system transfer function to eliminate the system imperfections.
- In ICARDS, usage of a Sensitivity Time Control (STC) resulted in the loss of layering information. This was solved by using two channels in ACORDS.
- The I-Q demodulator in ICARDS resulted in an imbalance in phase and amplitude of the I and Q channels, and this imbalance created an image signal that could limit the dynamic range of the receiver. In ACORDS, the digital down conversion of the return signal by bandpass sampling eliminates the use of the I-Q demodulator and the Local Oscillator.

## 3 Experiment Description and Signal Processing

---

The first part of this chapter explains the experiments conducted in Antarctica in the Austral summer of 2002 using the Improved Antarctic and Arctic Coherent Radar Depth Sounder (ICARDS) and in Greenland in the summer of 2003 using the Advanced COherent Radar Depth Sounder (ACORDS). The later part explains the signal processing performed on the data to improve the signal-to-noise-ratio and enhance the spatial resolution.

### 3.1 Measurements over Antarctica

In the Austral summer of 2002, radar measurements were made using ICARDS (described in the previous chapter) over the Peninsula, Pine Island and Thwaites glaciers (PIG/TG) in Antarctica. The field experiment included six flightlines (four missions in PIG/TG regions and two missions in the Antarctic Peninsula) in November – December of 2002. ICARDS was mounted on a Chilean Navy P-3 aircraft equipped with a Global Positioning System receiver and a laser altimeter to measure the surface elevation. The laser altimeter measures the elevation accurately to about 10 cm [7]. The GPS information is tagged with the thickness and elevation data to provide the geolocation of the measurements. The aircraft is usually flown between a speed of 130 m/s and 150 m/s and at altitude of 500 m to 1000 m

depending upon the weather conditions. Figure (3.1) shows the flightlines during the six missions.

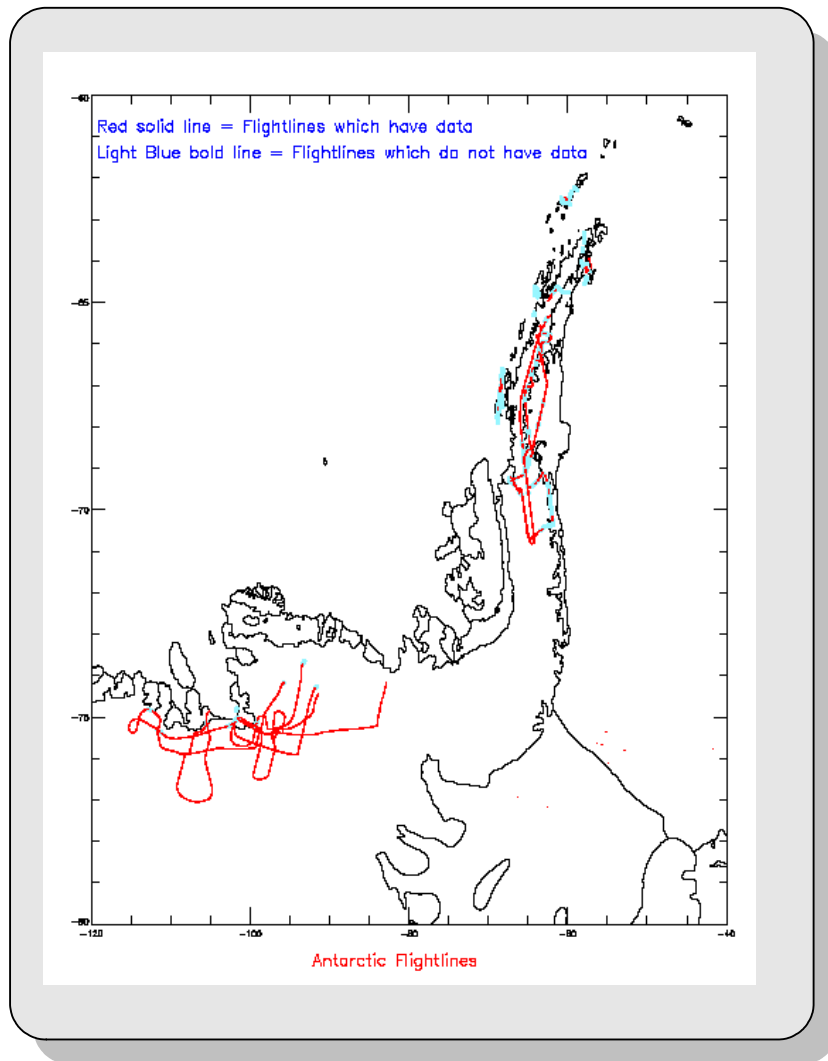


Figure 3.1: Flightlines of the Antarctic Mission, November – December 2002

### **3.1.1 Operation of Radar**

The radar operator sets several parameters on the data-acquisition software [8] before switching on the data system. The important parameters are briefly described here.

#### **3.1.1.1 Number of Samples**

The operator sets the *Number of Samples* depending upon the anticipated ice thickness. Each sample corresponds to 4.494 m of thickness in ice. Our system is capable of acquiring 1024 samples, which corresponds to about 4.5 km of ice thickness.

#### **3.1.1.2 Pulse Repetition Frequency**

The Pulse Repetition Frequency is selectable to 19.2 kHz.

#### **3.1.1.3 Number of Coherent Integrations**

Number of coherent integrations to be performed before data is stored.

#### **3.1.1.4 Number of Incoherent Integrations**

Incoherent integrations are done to display the real-time data only. Data is always stored in coherent mode only.

#### **3.1.1.5 Sample Window Delay**

The delay is set to begin recording the data samples just before the antenna feed through signal is received. This ensures that the data samples are not wasted in recording the internal feed-through signals from the radar.

The other system parameters are tabulated in Table (2.1) in chapter 2.

### 3.1.2 ICARDS Data File Structure

Once the raw data are collected, they are formatted into a specific file structure before they can be processed. This section describes the file format of the Antarctic data collected by ICARDS.

- The first 64 bytes of the data file is the *Header*, which is organized as shown in Table (3.1)

System Parameter	Type	Size (bytes)
Pulse Repetition Frequency (Hz)	Float	4
Sample Window Delay (seconds)	Float	4
DSP Mode	Unsigned Integer	4
Number of Samples	Unsigned Integer	4
Number of Coherent Integrations	Unsigned Integer	4
Number of Incoherent Integrations	Unsigned Integer	4
Number of Receiver Cards	Unsigned Integer	4
Data Format	Unsigned Integer	4
Fields 9 – 16: Blank	Unsigned Integer	4

Table 3.1: ICARDS Data Header Format

The common setting under which the radar was operated during the field experiment is described in Table (3.2).

<b>System Parameter</b>	<b>Value</b>
Pulse Repetition Frequency	9.2 kHz
Sample Window Delay	12 $\mu$ s
DSP Mode	0
Number of Samples	1024
Number of Coherent Integrations	128
Number of Incoherent Integrations	4
Number of Receiver Cards	1
Data Format	0
Fields 9 – 16: Blank	Unsigned Integer

Table 3.2: Radar Setting of ICARDS

- The header is followed by the measured data values. Each of these data is preceded by a header that describes the type of the data, size of the data and the number of records contained in the data. This is explained in the Table (3.3).

Data Type (4 bytes – Integer)	Data Size (4 bytes – Integer)	Number of Records (4 bytes – Integer)
Data		

Table 3.3: ICARDS Data Format

This format is repeated for all the data in the file.

- The data stored in this format can be accessed by specifying the data type.

The datatypes are described in Table (3.4).

Datatype	Parameter	Format
0	Header	16 Elements 4 Bytes Each
1	Incoherent Raw Data	2 Byte Unsigned Integer
2	I Channel Raw Data	2 Byte Integer
3	Q Channel Raw Data	2 Byte Integer
4	GPS String	1 Byte Unsigned Integer
5	System Time	1 Byte Unsigned Integer
20	Top Curve	4 Byte Float
21	Bottom Curve	4 Byte Float

Table 3.4: ICARDS Datatypes

The Figure (3.2) shows the radio echogram and the ice thickness profile along the Pine Island Glacier sounded by ICARDS.

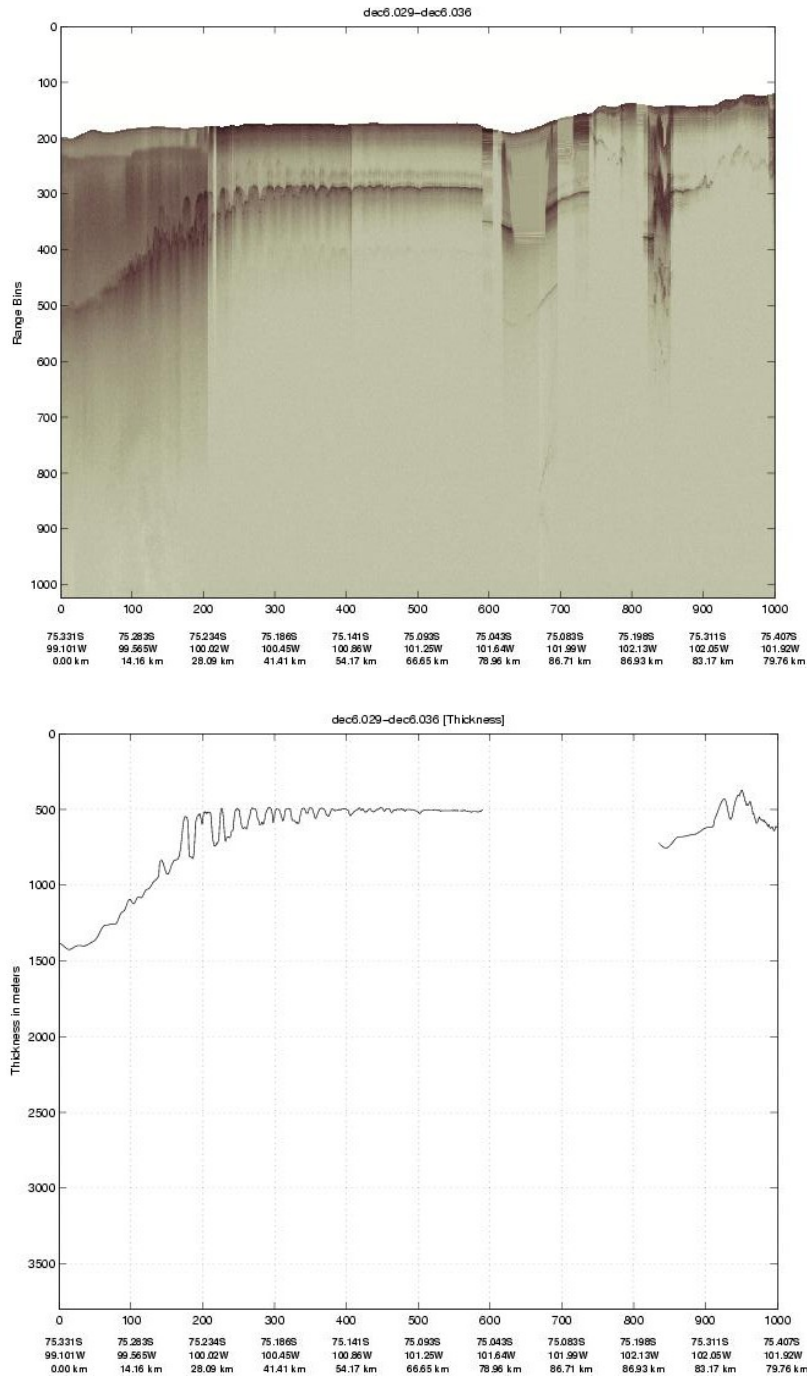


Figure 3.2: Radio Echogram and Thickness Profile along Pine Island Glacier

## 3.2 Measurements over Greenland

In the summer of 2003, radar measurements were made using ACORDS (described in the previous chapter) over the glaciers in Greenland. The field experiment included six flightlines in May 2003. Similar to the Antarctic mission, ACORDS was mounted on a NASA P-3 aircraft equipped with a GPS receiver and a laser altimeter. Figure (3.3) shows the flightlines during the six experiments.

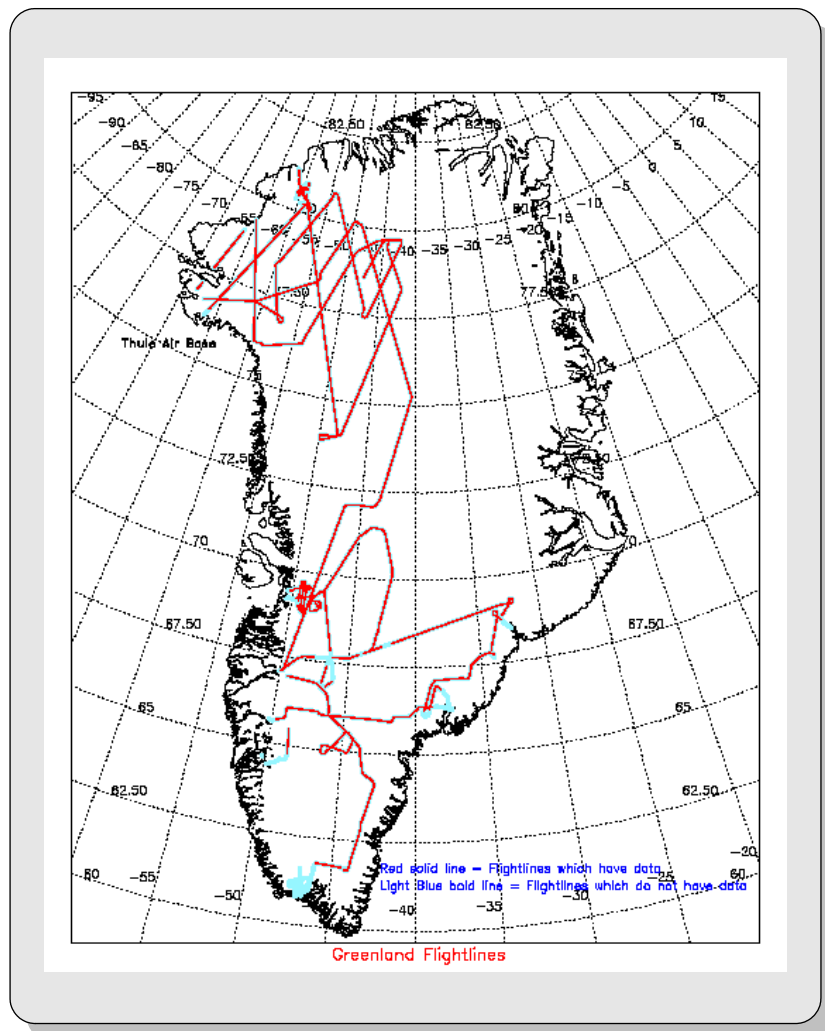


Figure 3.3: Flightlines of the Greenland Mission, May 2003

As discussed in the previous chapter, the return signal is amplified into two channels – a low gain and a high gain channel. The channels are operated by clock synchronized switches such that the stronger returns from the air/ice interface are received into the low gain channel and the weaker returns from the deeper layers and the ice/bed interface are received into the high gain channel. Saturation is prevented by adjusting the attenuation in the channels. The returns from the two channels are digitized at the rate of 55 megasamples per second. This digitized data is pre-integrated to reduce the volume of the data before storage. The number of coherent integrations is decided by the user depending upon the depth of ice being sounded.

### 3.2.1 ACORDS Data File Structure

The data collected by ACORDS are formatted into a specific file structure before any further signal processing is performed on the data. This section describes the file format of the Greenland data collected by ACORDS.

The stored data are accessed by specifying a data type (refer Table 3.5).

<b>Datatype</b>	<b>Parameter</b>
0	Header
1	Transmit Waveform
2	Data

Table 3.5: ACORDS Datatypes

A time tag that serves as an arbitrary time stamp for the collected data precedes each datatype. Table (3.7) describes the organization of the ACORDS data. The header is followed by the length of the transmit chirp and the transmit chirp value for the entire length. The low gain channel data and the high gain channel data are alternately stored for the entire length of the record. The entire data set is stored in the same format for all the records.

The common setting under which the radar was operated during the field experiment is described in Table (3.6).

<b>System Parameter</b>	<b>Value</b>
Pulse Repetition Frequency	9.2 kHz
Transmitted Pulse width	3 $\mu$ s
Transmit Chirp Weighting	Hamming
Receiver Blanking	0
High Gain Channel Blanking	8 $\mu$ s
Low Gain Channel Attenuation	36
High Gain Channel Attenuation	20

Table 3.6: Radar Setting of ACORDS

<b>System Parameter</b>	<b>Type</b>	<b>Size (bytes)</b>
Time Tag (s + $\mu$ s)	Integer	8
Number of Samples	Integer	4
Number of Pre-Integrations	Integer	4
Shift	Integer	4
Pulse Repetition Frequency	Double	8
Start Frequency	Double	8
Stop Frequency	Double	8
Waveform Generator Clock	Double	8
Under-sampling Clock	Double	8
Transmitted Pulse Width	Double	8
Transmit Chirp Weighting	Integer	4
Sample Window Delay	Double	8
Receiver Blanking	Double	8
High Gain Channel Blanking	Double	8
Low Gain Channel Attenuation	Integer	4
High Gain Channel Attenuation	Integer	4
Time Tag (s + $\mu$ s)	Integer	4
Length of Transmit Waveform (L)	Integer	4
Transmit Waveform	Short Integer	2 bytes each of length L
Time Tag (s + $\mu$ s)	Integer	8
Data	Unsigned Short Integer	2 bytes for each channel each of N samples

Table 3.7: ACORDS Data Format

Figure (3.4) shows the echogram and the thickness profile of the ice sheet near Petermann glacier.

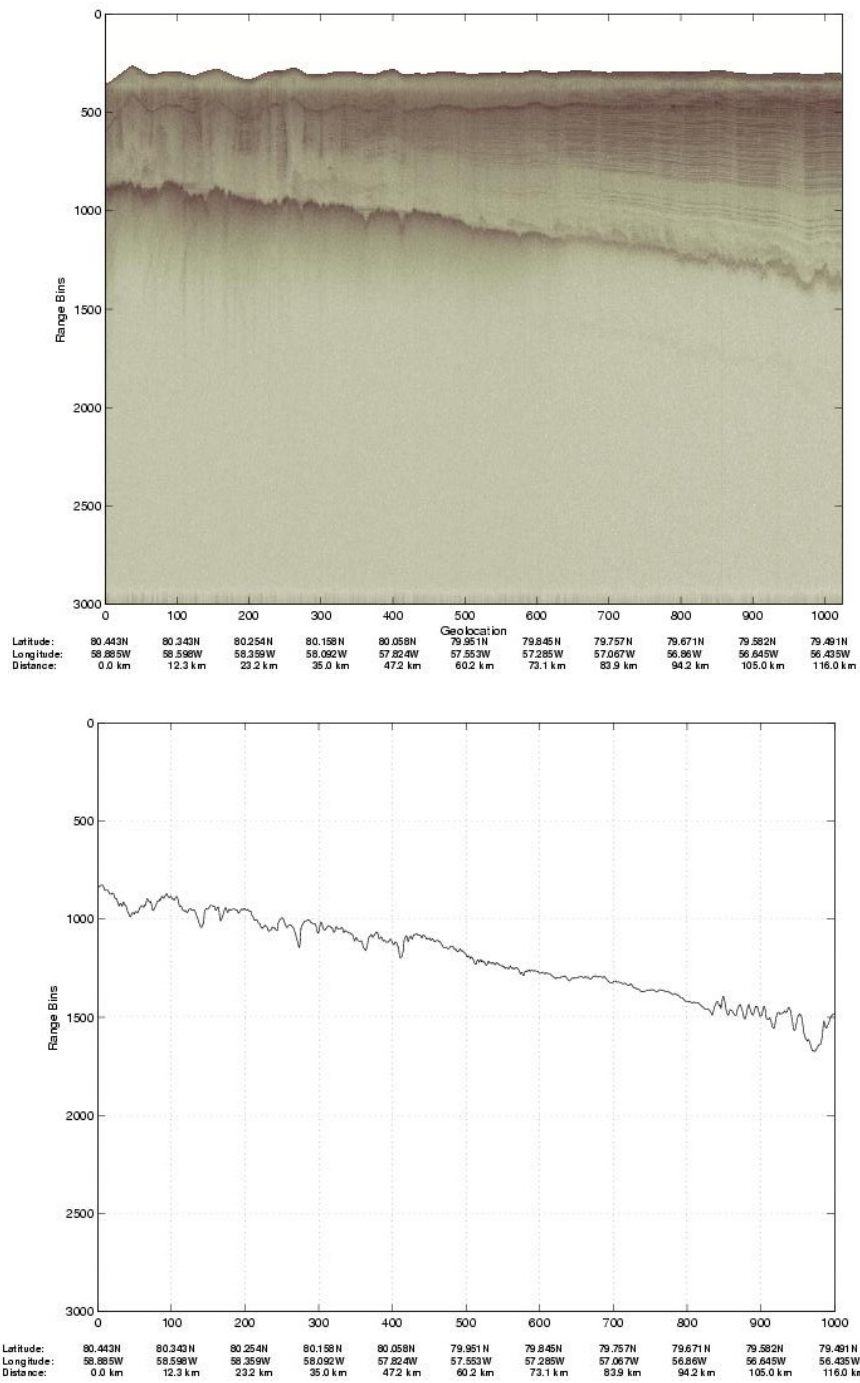


Figure 3.4: Radio Echogram and Thickness profile of ice sheet sounded near Petermann Glacier

### 3.3 Signal Processing

The collected and restructured data is further processed to enable accurate determination of ice thickness. The ice thickness is determined by computing the number of samples or range bins between the ice surface and the ice/bedrock interface and multiplying this by the range resolution of the radar.

#### 3.3.1 Pulse Integration: Software

Pulse integration is the process of adding radar returns from many pulses. Coherent integration has a twofold effect on the radar signal. It reduces the random noise and enhances the spatial resolution by synthesizing a longer antenna (unfocussed SAR), which in turn reduces the beamwidth of the antenna. When the pulses are added prior to detecting the envelope of the return signal, the return pulses get *coherently* added and so the phase relationship between them is preserved. When the envelope of the return pulses is detected, the phase relationship between the pulses is lost. This is called *incoherent integration*.

 samples are coherently integrated, it results in an SNR gain of  $N$  dB, and if  $N$  samples are incoherently integrated, there is an SNR gain of  $\sqrt{N}$  dB [9].

Figure (3.5) illustrates the effect of integrating the pulses. The figure shows the normalized return power (in dB) as a function of the range cell for measurement over West Greenland using ACORDS. The return power after 10 coherent and 4

incoherent integrations is shown in red. It can be seen that there is a reduction in the noise floor after pulse integration.

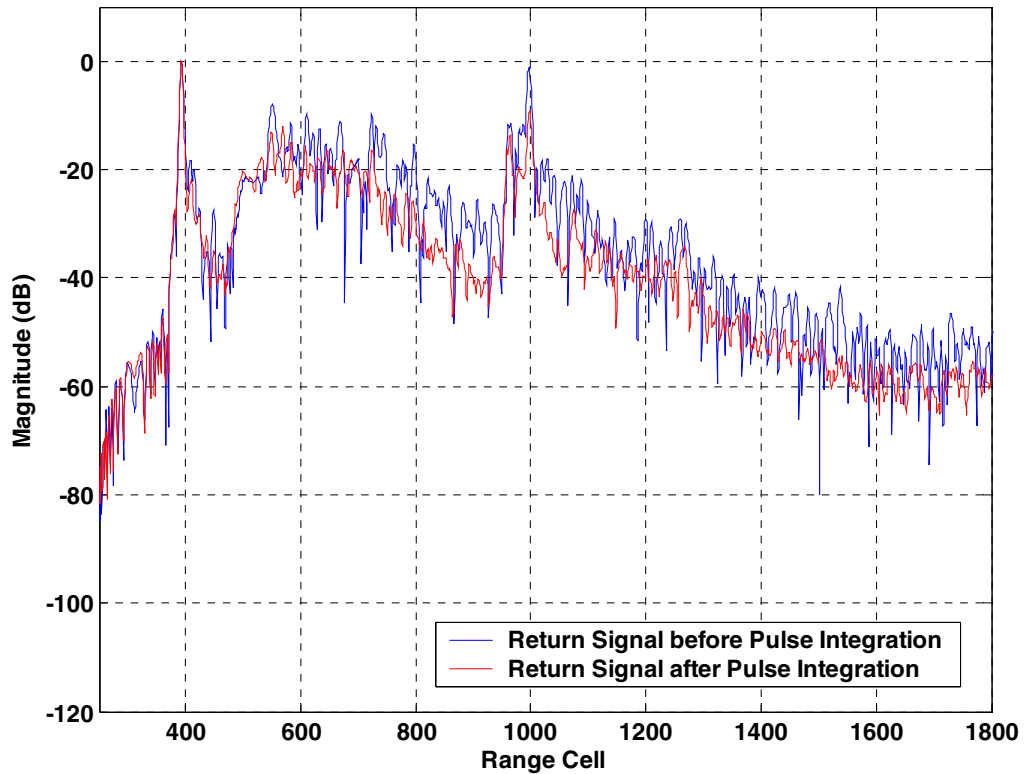


Figure 3.5: Result of Pulse Integration

### 3.3.2 D.C.Offset Removal

The radio frequency power that leaks through the RF switches, power supply lines, etc., to the antenna and gets transmitted during the off period of the transmitter is called D.C offset. This leakage will translate into a significant signal at the receiver

output owing to the high receiver gain. DC offsets are eliminated from the data by determining the mean level of the noise floor in each A-scope and subtracting it from the return signal from the ice layer.

If  $nS$  is the number of samples (or range cells) at the end of each A-scope considered as noise, then the average noise level  $N_{Ave}$  is given by

$$N_{Ave} = \left[ \frac{\sum^{nS} N}{nS} \right]$$

This is subtracted from the return signal from the ice layer.

$$\tilde{S} = S - N_{Ave}$$

### 3.3.3 Gain Compensation

The noise power level in the return data is normalized to remove any sudden increase in the noise level. The changes in noise levels are usually due to changes in the receiver gain. The operator changes the gain of the receiver depending on the terrain over which the radar is flown. The process of normalizing the gain is called gain compensation or gain equalization. The average noise power level of the return pulses received in one-second duration is determined. The gain compensation factor in the one-second window is calculated as the ratio of this maximum average noise level (calculated above) to the average noise level of the pulses received in one-second

duration. The gain of the pulses received from the ice layers is normalized using the corresponding gain compensation factor. This is mathematically illustrated below:

If  $PRF$  is the pulse repetition frequency and  $nCoh$  denotes the number of coherent pre-integrations performed on the return signal, then the number of pulses returned in one second is given by  $nP$  as

$$nP = \frac{PRF}{nCoh}$$

If  $nS$  is the number of samples (or range cells) at the end of each A-scope considered as noise, then the average noise power level in one-second duration is

$$P_{N-Ave} = \frac{1}{nP} \sum_1^{nP} \left[ \frac{\sum_1^{nS} P_N}{nS} \right]$$

where  $P_N$  is the noise power level. The maximum average noise power level is

$$P_{N-Max} = \max((P_{N-Ave})_{1...K})$$

$$k = nR / nP$$

where  $nR$  is the total number of records.

The gain compensation factor for each one-second window is

$$\rho_{1...k} = \sqrt{(P_{N-Max} / P_{(N-Ave)_{1...k}})}$$

The return signal from the ice sheet is gain compensated using the corresponding value of  $\rho$ .

$$\tilde{S} = S_{1\dots k} \times \rho_{1\dots k}$$

Figure (3.6) illustrates the effect of gain compensation using a radio echogram from Pine Island Glacier from the measurements taken by ICARDS. In the upper part of the figure, the return from the ice/bedrock interface becomes almost invisible in the latter half of the echogram. The lower part of the figure shows the echogram after the gain in the data is equalized and DC offset has been removed. It can be observed that the return from the ice/bedrock interface is clear in the latter half of the echogram, and some of the internal layers are also distinctly visible.

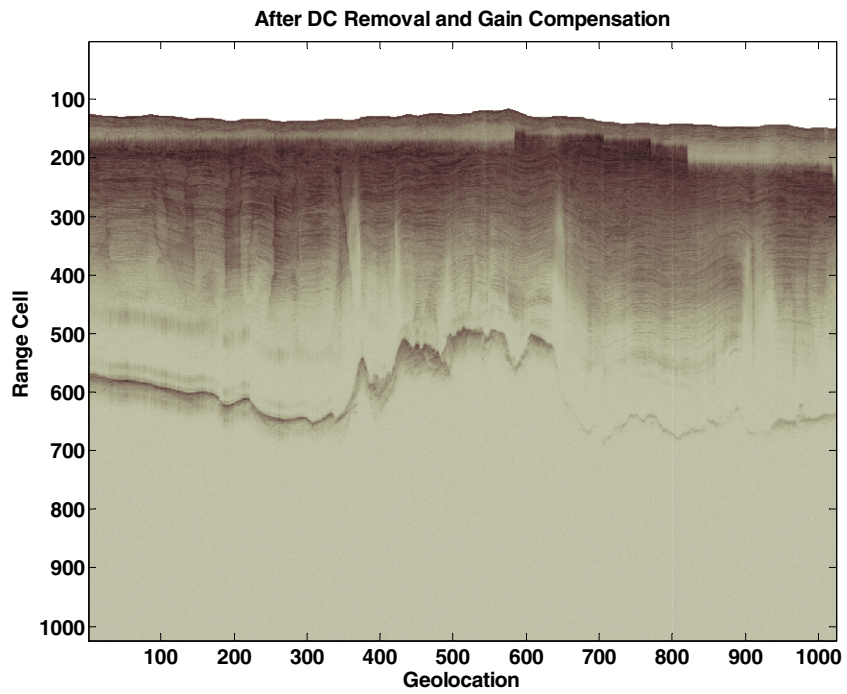
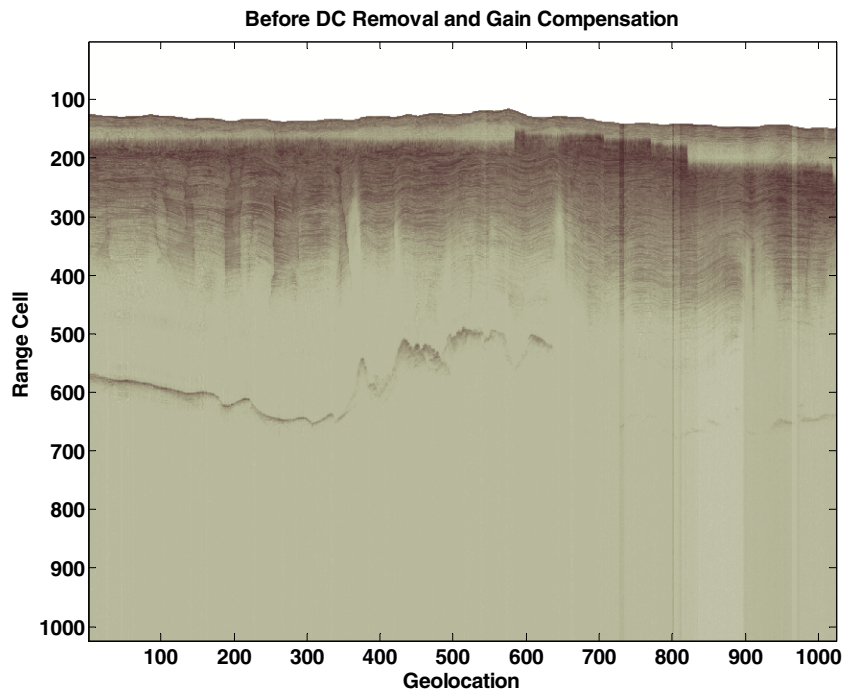


Figure 3.6: Radar Echogram of the Pine Island Glacier illustrating the effect of gain compensation

### 3.3.4 Coherent Noise Reduction

Coherent noise in the return signal is the result of reflections and leakage signals from the antenna and the RF section [10]. These undesirable components of the return signal have phase continuity with the backscattered signals from the glacial ice. To obtain accurate measurement of the backscattered echoes, it is critical to reduce coherent noise as much as possible.

Signals from systematic sources such as antenna and the RF section vary spatially and temporally, but the signals from distributed targets such as the backscattered echoes from the ice sheet vary with time and not with space. This fact is exploited in reducing the coherent noise.

The coherent noise component in each record is estimated by coherently averaging the return signal received over a considerably long time duration (for example, 12 to 15 seconds). The time duration over which the return signal is averaged should be long enough to decorrelate the backscattered pulses. The coherent noise is then subtracted from the return signal.

Figure (3.7) shows the return signal from the high gain channel before and after coherent noise reduction. The coherent noise in the channel has been reduced by about 15dB.

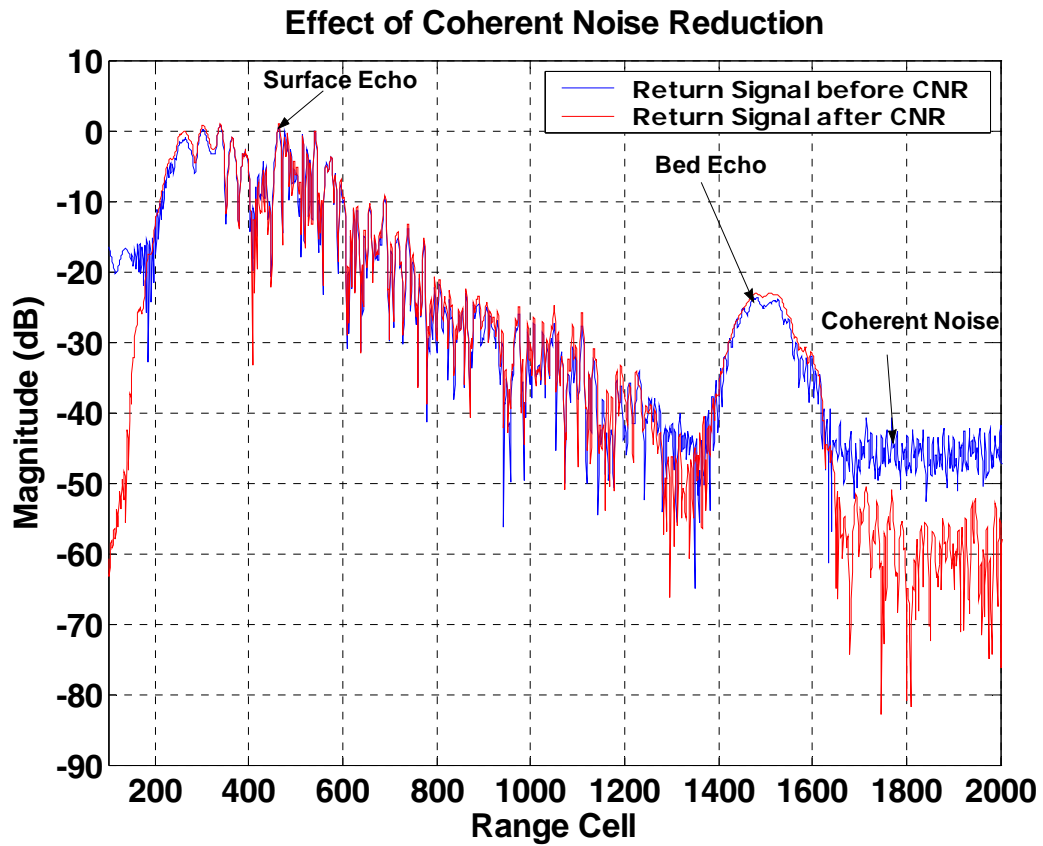


Figure 3.7: Return Signal measured by ACORDS near Humboldt Glacier: Result of Coherent Noise Reduction

Figure (3.8) shows the noise spectrum of the return signal in the high gain channel. The upper part of the figure shows the spectrum prior to coherent noise reduction. The spikes in the spectrum have been greatly reduced in the lower part of the figure by reducing coherent noise.

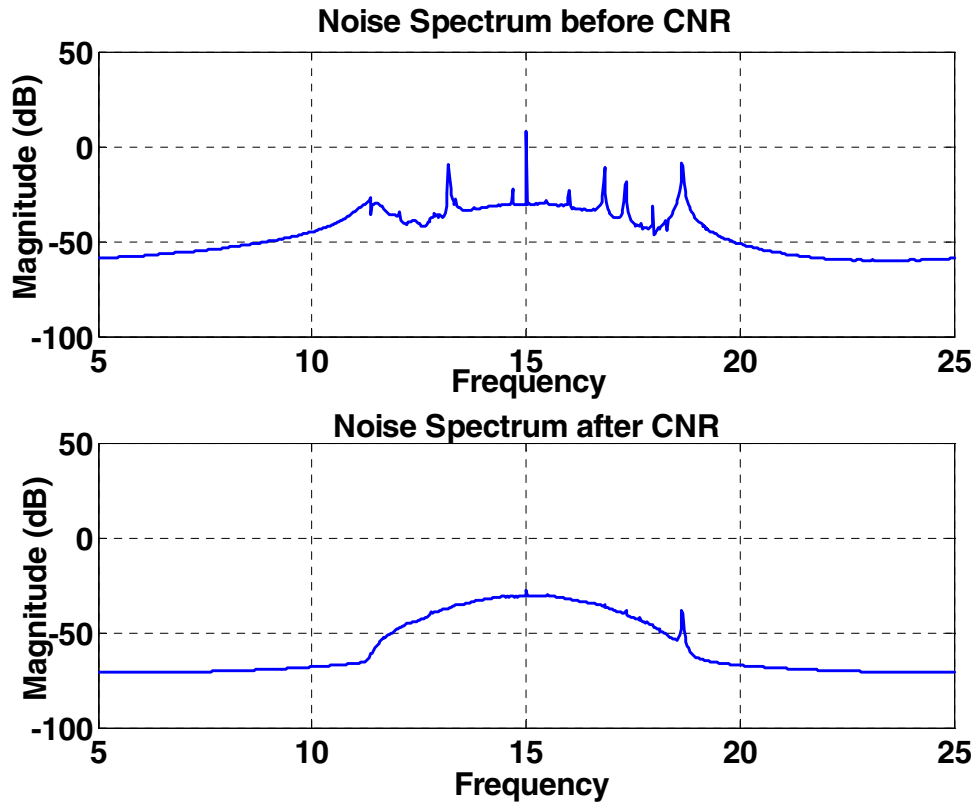


Figure 3.8: Noise Spectrum in the High Gain Channel

### 3.3.5 Multiple-Echo Cancellation

*Multiple Echoes* are undesirable components of the return signal resulting from the multipath phenomenon involving reflections from the ice surface and the bottom of the aircraft. The range at which the first multiple reflection is observed corresponds to the height of the aircraft above the air/ice interface. Eliminating the multiple-reflection is very critical in the regions where the depth of the ice sheet below the surface is about the same as the height of the aircraft above the surface. In such cases,

the multipath components occur at the same range as the return from the ice/bed interface, thus masking the bed echo and impairing accurate measurement of ice

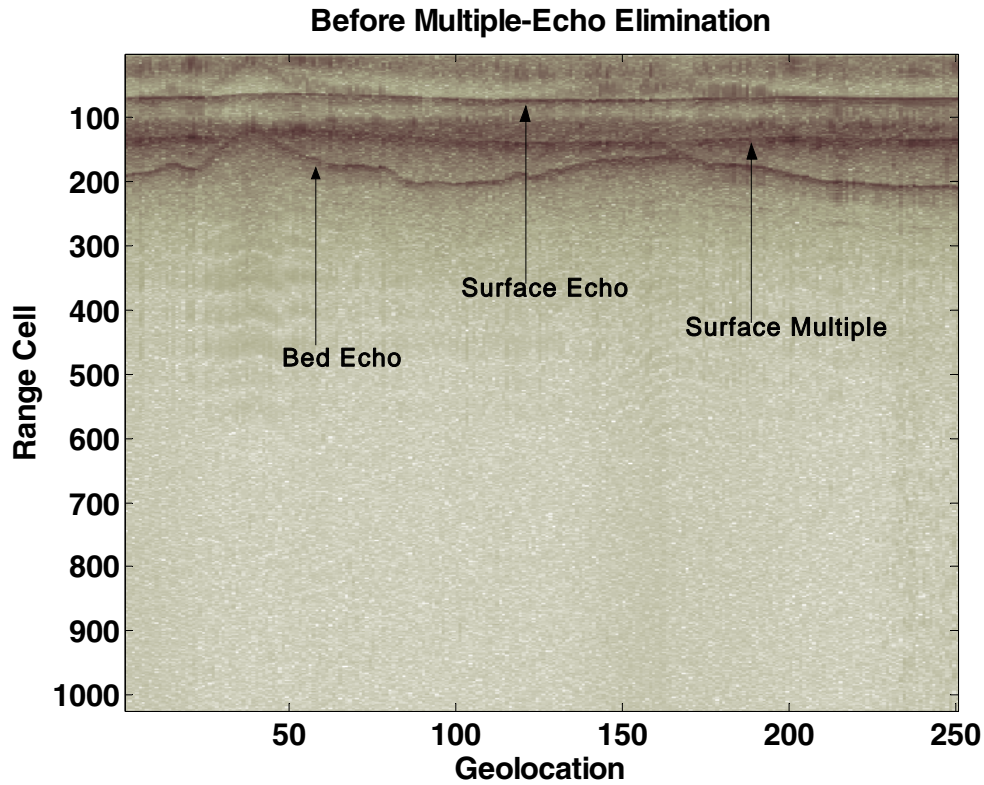


Figure 3.9 a: Echogram illustrating Multiple Echo

thickness. Figure (3.9 a) shows an echogram of the radar return measured by ICARDS. The first order surface multiple is partially masking the return from the bedrock in certain A-scopes.

The algorithm for eliminating the multiple echo is described below:

- The position of the aircraft (transmitter and receiver) above the ice surface is determined by locating the range cell at which the antenna feed through occurs. Antenna feed through is the leakage signal from the transmitter to the receiver.
- The range cell at which the return from the air/ice interface occurs is located. The difference between this and the range at which the antenna feed through occurs is an estimate of the aircraft altitude.
- As discussed earlier, the first order multiple occurs at the same depth below the air/ice interface as the height of the aircraft above the air/ice interface. Using this fact, an approximate position of the multiple is determined.
- The amplitude and phase of the multiple echo is determined from the amplitude and phase of the maximum peak in a small region around the range cell determined from the above step.
- A replica of the multiple is synthesized by filtering out the return from the air/ice interface using a 5<sup>th</sup> order Butterworth filter and injecting the filtered return with the phase of the multiple echo and scaling down its amplitude to the amplitude of the multiple-echo.
- This synthesized signal is subtracted from the actual return signal to eliminate the multiple-echo.

The result of multiple echo cancellation is shown in Figure (3.9 b).

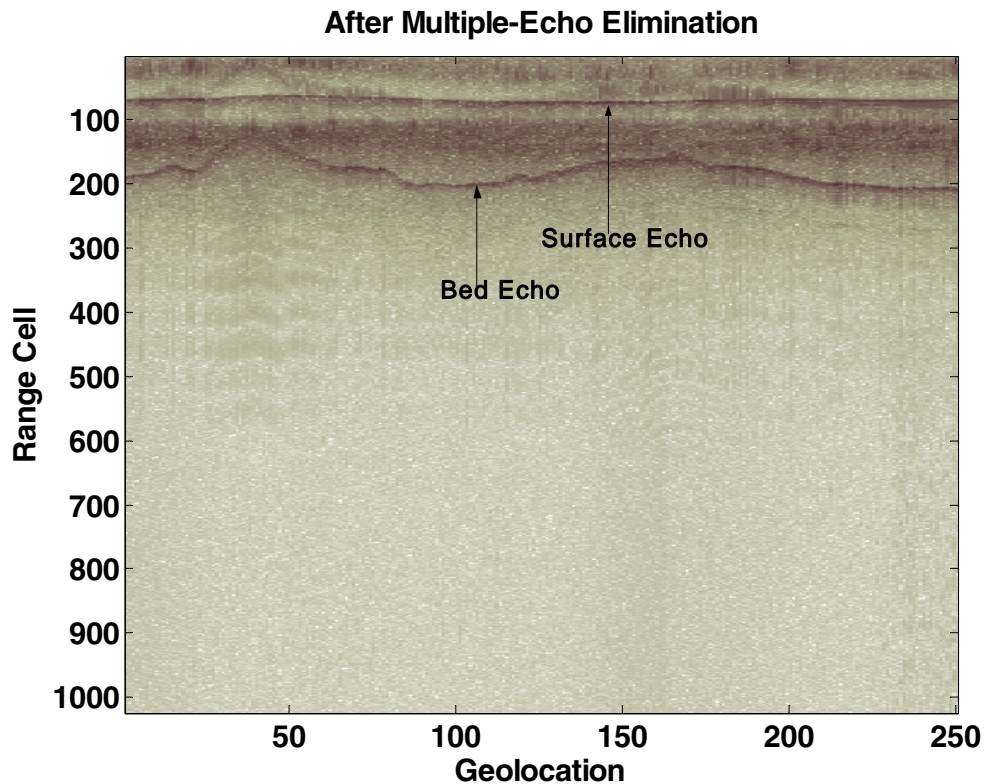


Figure 3.9 b: Multiple-echo has been eliminated, making the interpretation of the echo from the bedrock easier

### 3.3.6 Inter Gain Compensation

The preceding sections described the additional signal processing done on a single data file to enable accurate thickness measurement. Inter gain compensation is the same as gain compensation (see 3.3.3 above), and it compensates for the changes in the radar gain settings across adjacent data files.

The data collected by the depth sounder have been processed to obtain the thickness. These thickness data are modeled to generate a three-dimensional image of the

bedrock. The next chapters gives an overview of the image processing concepts involved in producing a raster from a data set of non-uniformly sampled points and displaying the raster in a three-dimensional perspective. The subsequent chapter describes the approach to interpolating the thickness datasets from outlet glaciers into a raster thickness model.

## 4 Data Interpolation

---

This chapter describes the basic principles behind data interpolation and describes the tool used to display the modeled data in a three-dimensional perspective. Data that have been collected and processed to evaluate the thickness of the ice sheet are to be modeled suitably before the topography of the bed can be displayed as a three-dimensional image.

### 4.1 Interpolating the Thickness Data

*Interpolation* converts the irregularly spaced samples collected over a continuous surface to create a grid (in the present case, the continuous surface is the bed of a glacier). It is impractical for any experiment to obtain the data from every location and hence at locations where data were not collected, a value is predicted from the dispersed samples. Interpolation creates a grid or a “raster” of the attribute that is being modeled from a limited number of sample data values, as shown in the example in Figure (4.1). A raster can be defined as an array of equi-spaced pixels that on the whole represents an image. On the left is the sampled data set and the interpolated grid is on the right. The input points from the sampled data set are weighted and the data values at the unknown locations are determined using a formula depending on the type of interpolation used.

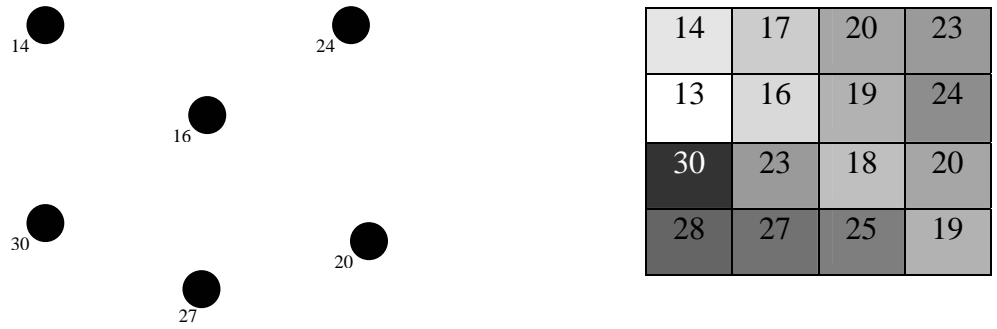


Figure 4.1: Interpolation of Discontinuous Samples into Raster

#### 4.1.1 Types of Interpolation

All the methods of interpolation operate on the assumption that the points that are close together tend to have similar characteristics, i.e., the points exhibit spatial correlation. It should be noted that when the irregularly sampled data sets are interpolated into rasters or grids to obtain surfaces of continuous data, the information about the sampled data set is degraded to some extent. This distortion of the information provided by the sampled data set is kept to a minimum by choosing the most suitable method of interpolation that minimizes the error between the predicted (interpolated) sample and the collected sample.

There are two types of interpolation, namely, *deterministic interpolation* and *geostatistical interpolation*. In the deterministic method, the surrounding points are weighted depending upon their distance from the prediction location to predict the

data value at the unknown location. On the other hand, the geostatistical method of interpolation takes into account the statistical relationship between the sampled points along with their distance from the prediction location to determine the weights.

### 4.1.2 Kriging Interpolation

Spatial correlation between the neighboring attribute values is an important characteristic of any geographical phenomenon. Similarly, the thickness measurements of ice sheets in the outlet glaciers exhibit spatial relationship to a great extent. Hence the ice thickness data in the outlet glaciers are modeled by a geostatistical interpolation technique called *kriging*. This method assumes that the distance or direction of the sample points reflects a spatial correlation that can be used to explain the variation in the surface. The weights to the sample points surrounding the prediction location are assigned on the basis of a least squares model fitted to the function representing the spatial variation in the data.

The general formula for kriging interpolator is given by

$$\hat{Z}(s_0) = \sum_{i=1}^N \lambda_i Z(s_i)$$

where  $Z(s_i)$  is the measured value at the  $i^{th}$  location,  $\lambda_i$  is the unknown weight for the measured value at the  $i^{th}$  location,  $s_0$  is the prediction location and  $N$  is the number of measured values. The weight  $\lambda_i$  depends on a model fitted to the measured samples,

the distance of the measured points from the prediction location and the spatial relationships among the measured values surrounding the prediction location.

### **4.1.3 Kriging – Procedure**

This section describes the various steps involved in interpolating the measured data points into a raster using the kriging interpolation method.

- **Calculating the Empirical Semivariogram**

Kriging, as discussed earlier, exploits the fact that the points that are close to one another are more similar than those that are farther apart. An empirical semivariogram is a tool that quantifies this fact. It is a plot of half the squared difference in the thickness values between all pairs of the measured sample points against the distance that separates these points. Hence the pairs of location that are on the far left on the x-axis would have a lower value on the y-axis, that is, they will be more spatially correlated. As we move along the x-axis, the spatial correlation between the pairs of points decreases (they tend to have a higher value on the y-axis).

- **Fitting a Model to the Empirical Semivariogram**

A model is fit to the points created in the empirical semivariogram above. This model, called a *Semivariogram*, is a weighted least squares fit and quantifies the spatial autocorrelation of the thickness data for all possible directions and distances.

The main characteristics that describe the semivariogram are *range*, *sill* and *nugget*. They are described in Figure (4.2). Range is the distance between two measured samples beyond which they are not spatially related. The value at which the range is attained is called the sill. At a very small distance between two samples, the semivariogram has a very small value (instead of zero) and this is called the nugget effect. This is due to spatial variation at distances less than the sampling interval or due to errors in the measurement or both. Partial sill is the difference between sill and nugget.

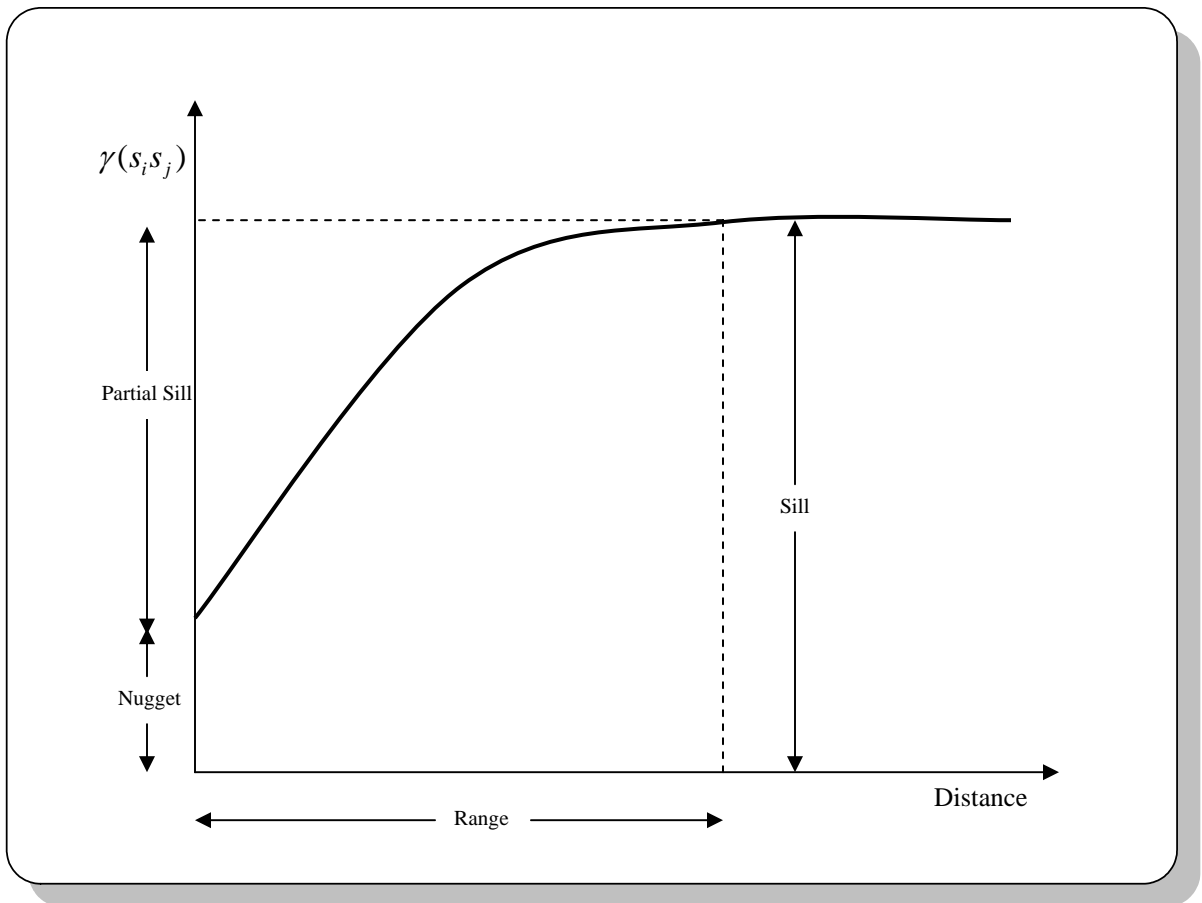


Figure 4.2: A Semivariogram

For example, the semivariogram describing the spatial dependence of thickness data collected over Jakobshavn Isbrae is shown in Figure (4.3). The plot has averaged semivariogram values on the y-axis and distance on the x – axis. It can be seen

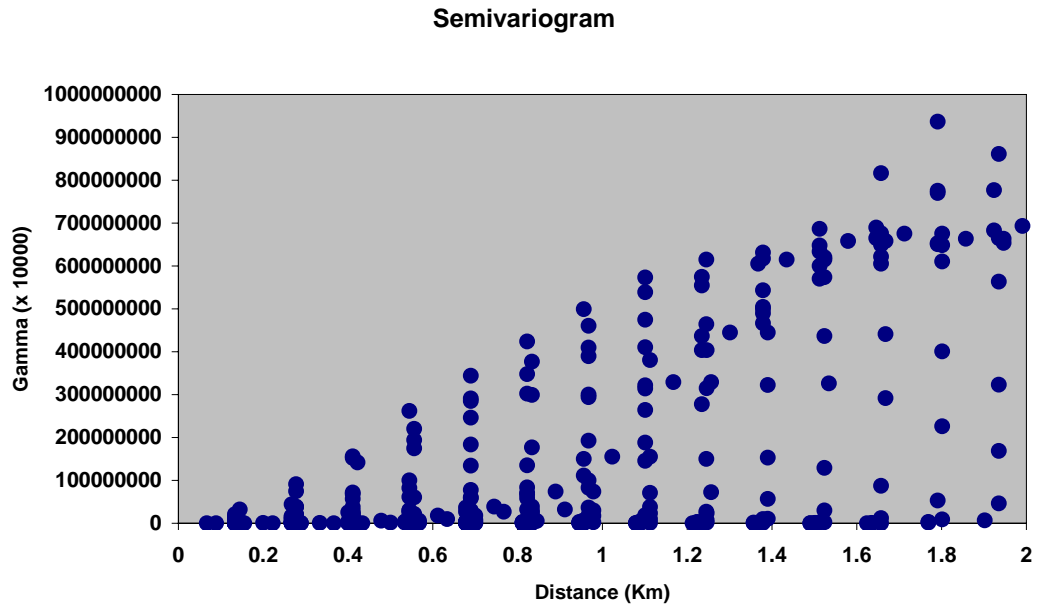


Figure 4.3: Semivariogram of Data over Jakobshavn

from the plot that the points that are separated by larger distances have less spatial correlation. An exponential model is fit to the distribution above as the spatial correlation decreases exponentially with increasing distance.

The semivariogram model should account for *anisotropy* in the measured data. The data is considered anisotropic because two points separated by a certain distance

might be spatially correlated to the same extent in one direction as two points separated by a different distance in another direction.

In the current scenario where measurements taken over a long period of time are used to fit a model that quantifies the spatial correlation observed along a surface, it is possible to encounter several differing observations at the same location. So prior to creating the weight matrices for prediction, any such variation (called *microscale variation*) and errors due to measurements have to be reduced so that if data are predicted using the weights created from the model, at a location where data are available, the predicted value should be as close to the measured value as possible. This is achieved by including a measurement error term in the model.

- **Validating the Model**

The model selected to fit the semivariogram influences the prediction of the unknown values. The model is chosen such that it best fits the semivariogram values so that there is only a minimal error in estimating the spatial autocorrelation. The model should be unbiased and the predicted values should have the correct variability from the true values.

The selected model is validated by analyzing the magnitude of errors between measured and predicted values. A “measured” data location is chosen and its value is “predicted” using the neighboring values on the basis of the designed interpolation

model. The predicted value is then compared with the measured value. This procedure is repeated for all the points. A validation model is created on the basis of these comparisons.

The model can be considered to be unbiased if the mean prediction error is close to zero. The root-mean-squared error is used as an important factor to validate the prediction model. RMS error is defined as the square root of an average squared difference between the measured and predicted values. The variability of the predicted values can be estimated from the average standard errors and the root-mean-squared error. For the predicted value to have the correct variability, the average standard error should be close to the root-mean-squared error.

- **Creating the Weight Matrices**

Matrices of the kriging weights to be assigned to the measured values to predict an unknown value in a neighborhood are calculated from the semivariogram.

The number of measured values to be included in predicting the weights is also obtained from the semivariogram. When handling large amounts of data, pairs of measured values are grouped based on their similarity in the distance from the prediction location and their average distance, and the semivariogram is plotted. This enhances the clarity in interpreting the semivariogram plot. There is a specific distance of separation between the prediction location and a measured value beyond

which there is no considerable autocorrelation, as evident from the semivariogram plot. The points within this distance are selected in predicting the weights.

- **Making the Prediction**

An unknown thickness sample is predicted using the weight matrices created using the estimate of the spatial autocorrelation.

## **4.2 Tool Used**

*ArcGIS* is an integrated geographic information system package and is used to create the raster thickness models, optimize the model and analyze the interpolated model [11]. The *arcGIS* package consists of several modules and extensions. The data are interpolated into a raster using *ArcGIS 3D Analyst* and displayed using *ArcScene*. *ArcScene* uses the pixel values stored in the raster to display it in a three-dimensional perspective. Three-dimensional display helps in visualizing the real-world features of the glaciers, such as the actual depth of the bedrock.

The bed topography of outlet glaciers is referenced to its geographical surroundings before they are displayed. This is called geo-referencing and is done by projecting the data to a reference geographical coordinate system in which the majority of measured data are located.

The next chapter describes the interpolation approach for the outlet glaciers. For each glacier data set, the interpolation approach has been assessed, validated and reasoned out as to why the specific approach gives the best-predicted result.

## 5 Implementation And Results

---

Ice thickness data collected over the past seven years by radar depth sounder systems have been used to generate three-dimensional images of the bed topography and digital thickness maps of three outlet glaciers – Petermann, Kangerlussuaq and Jakobshavn Isbrae. This chapter discusses the approach to obtaining the digital thickness raster for each of these glaciers, validation of the approach and the results of the implementation.

### 5.1 Kangerlussuaq Glacier

The flightlines along which measurements were made over Kangerlussuaq Glacier (68.7°N 33.3°W) from 1998 to 2003 are shown on the left side of Figure (5.1). The radar data collected by ACORDS in 2003 over this region have been processed for thickness measurement and integrated with data points collected over the previous years. Data at the center of the glaciers are denser than those at the edges. So when the data set is interpolated into a raster, the predicted values at the center will be closer to the true values than those at the edges. Average spacing of the data is about 130 m. Some of the data collected along the flight turns were filtered out before performing interpolation. They were filtered out to avoid any error in the actual thickness values because of the flight banking in the turns. The filtered dataset, shown on the right side of Figure (5.1) was then interpolated into a raster.

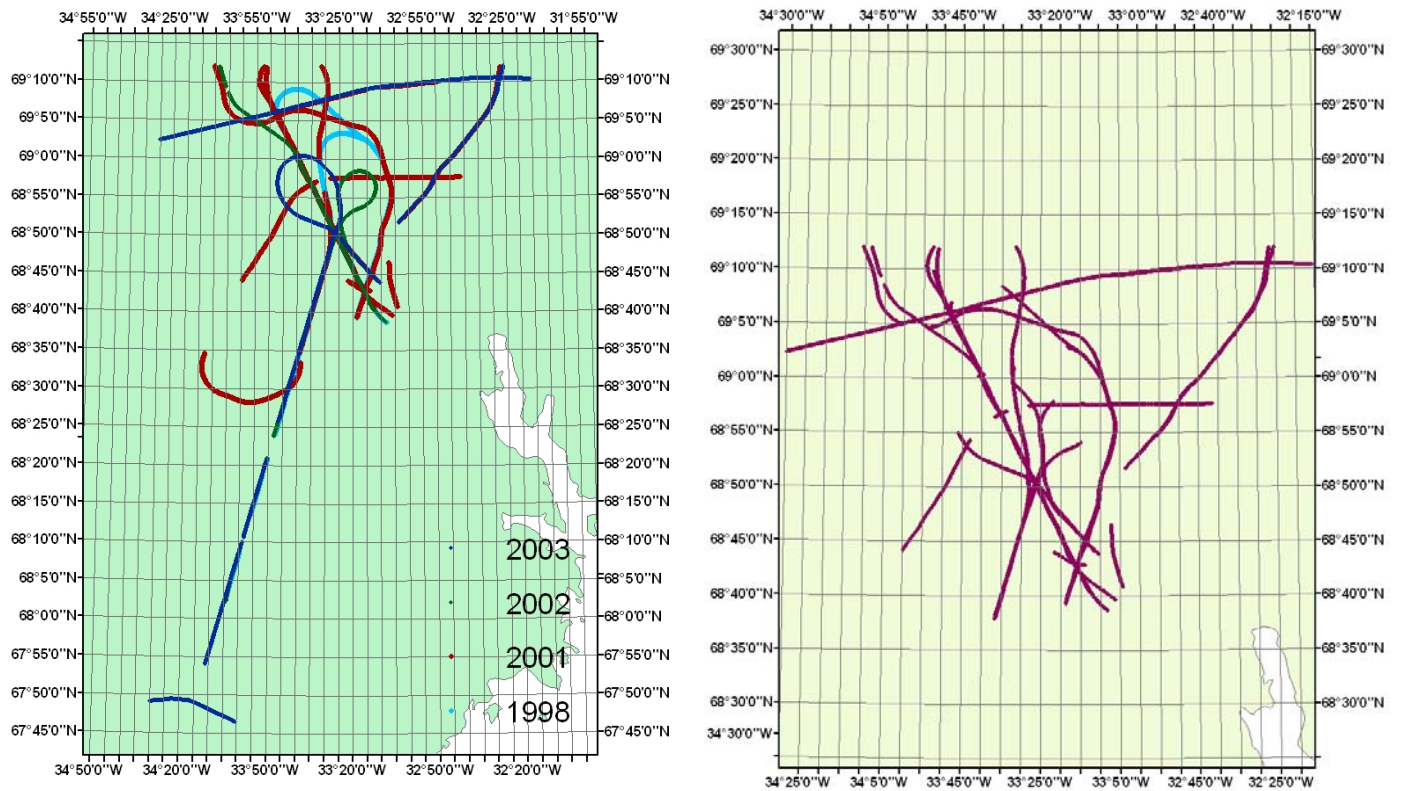


Figure 5.1 a: Flightlines over Kangerlussuaq

In Figure (5.1 b) the integrated and filtered flightlines are shown on a high-resolution ASTER (Advanced Spaceborne Thermal Emission and Reflection Radiometer) image obtained from [6] to interpret the ice thickness measurements with respect to the ice sheet flow lines. The thickness profiles for some major flightlines are also shown.

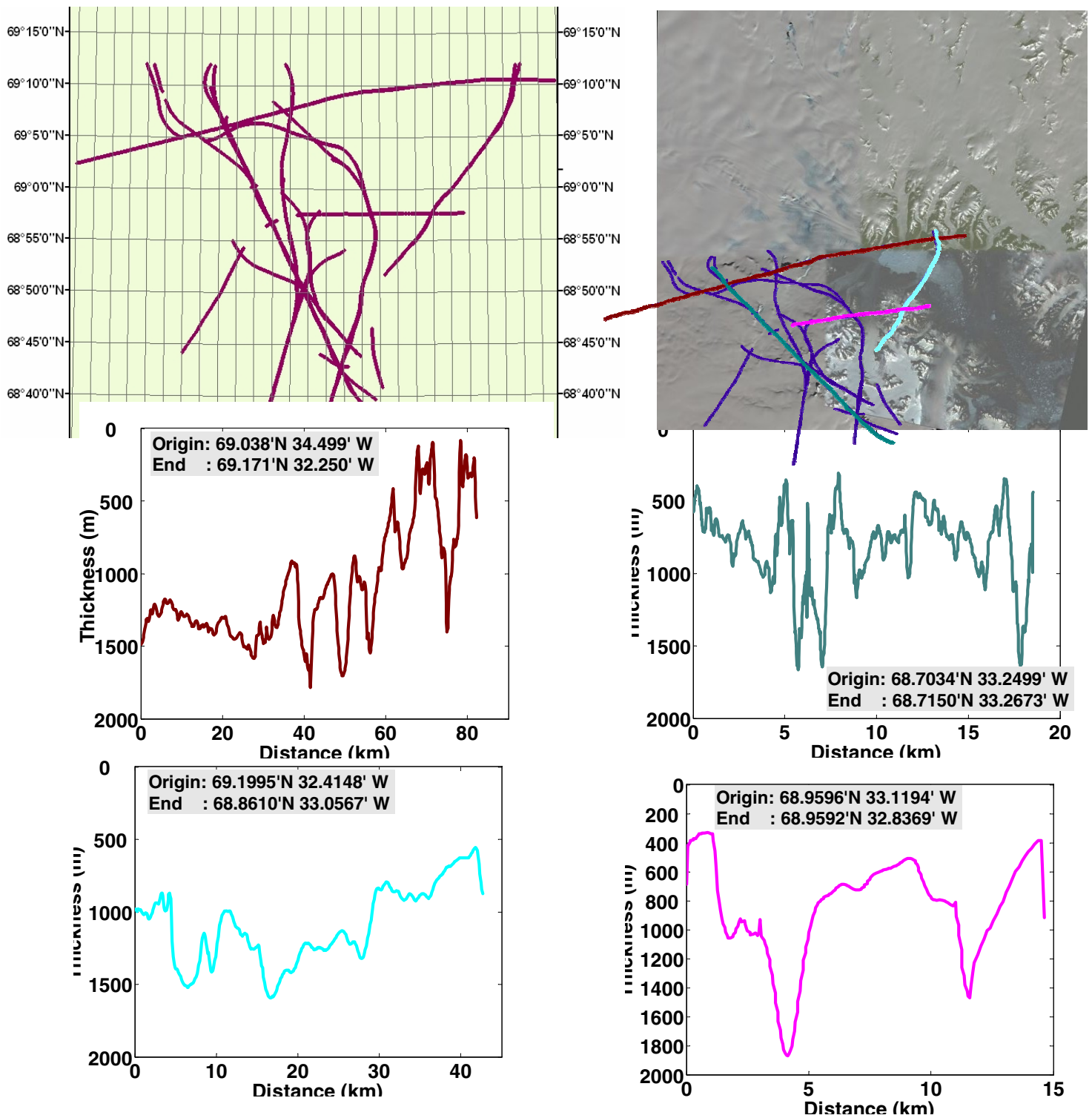


Figure (5.1 b) Kangerlussuaq Flightlines on a High Resolution Image of the Glacier and thickness profiles of major flight paths

### **5.1.1 Interpolation to Raster Thickness Data**

The measured thickness data is interpolated by kriging to a raster in a two-step process. Firstly, the spatial correlation among the values is quantified, and depending upon the estimated statistical dependence among the values, the interpolation model is designed. Secondly, this model is implemented on the data to create the raster.

#### **5.1.1.1 Design**

As discussed in the previous chapter, plotting the empirical Semivariogram and fitting a least squares model to it uncovers the spatial dependency among the thickness values. It is observed that exponential and spherical models for the spatial autocorrelation function were the best fit for the thickness data of all the three outlet glaciers.

The semivariogram plot of Kangerlussuaq glacier was fit with an exponential curve since the autocorrelation decreased exponentially with increasing distance. The sill was found to be 158.179 km. The spatial dependence between points is negligible beyond this distance. Anisotropy and nugget effect are accounted for in the model. Since there are overlapping data, the measurement error model is included.

### **5.1.1.2 Validation**

As discussed earlier, for the thickness dataset, spherical or exponential curve was found to have the minimum deviation from the values in the Semivariogram. So the interpolation is modeled with spherical and exponential fits and validated.

For interpolating the thickness data over Kangerlussuaq into a raster, an exponential model was clearly the most suitable as it had almost a zero mean prediction error (0.0004), compared to 0.003 for the spherical model. This shows that the exponential model was an unbiased method of prediction.

### **5.1.1.3 Implementation**

The values of the parameters (nugget, sill and range) obtained from the design are used to create the weight matrix using the exponential fit. Each unknown value is determined using twelve neighboring measured values. So the radius within which the measured points are weighted is varied so as to include twelve neighboring points in the interpolation. The size of each cell of the output raster determines the resolution of the image. The output raster of Kangerlussuaq is constructed with a cell size of 100 m, which is finer than the input cell. Specifying a lesser value for the output cell results in a very rough image. In addition, the size is also bound by hardware limitations as the interpolation becomes complex when the ratio of input to output cell size becomes large.

#### 5.1.1.4 Results

The raster resulting from the interpolation method implemented above is displayed as a 3-dimensional image as shown in Figure (5.2 a). The image is plotted on a different color spectrum in Figure (5.2 b) to interpret finer changes in thickness.

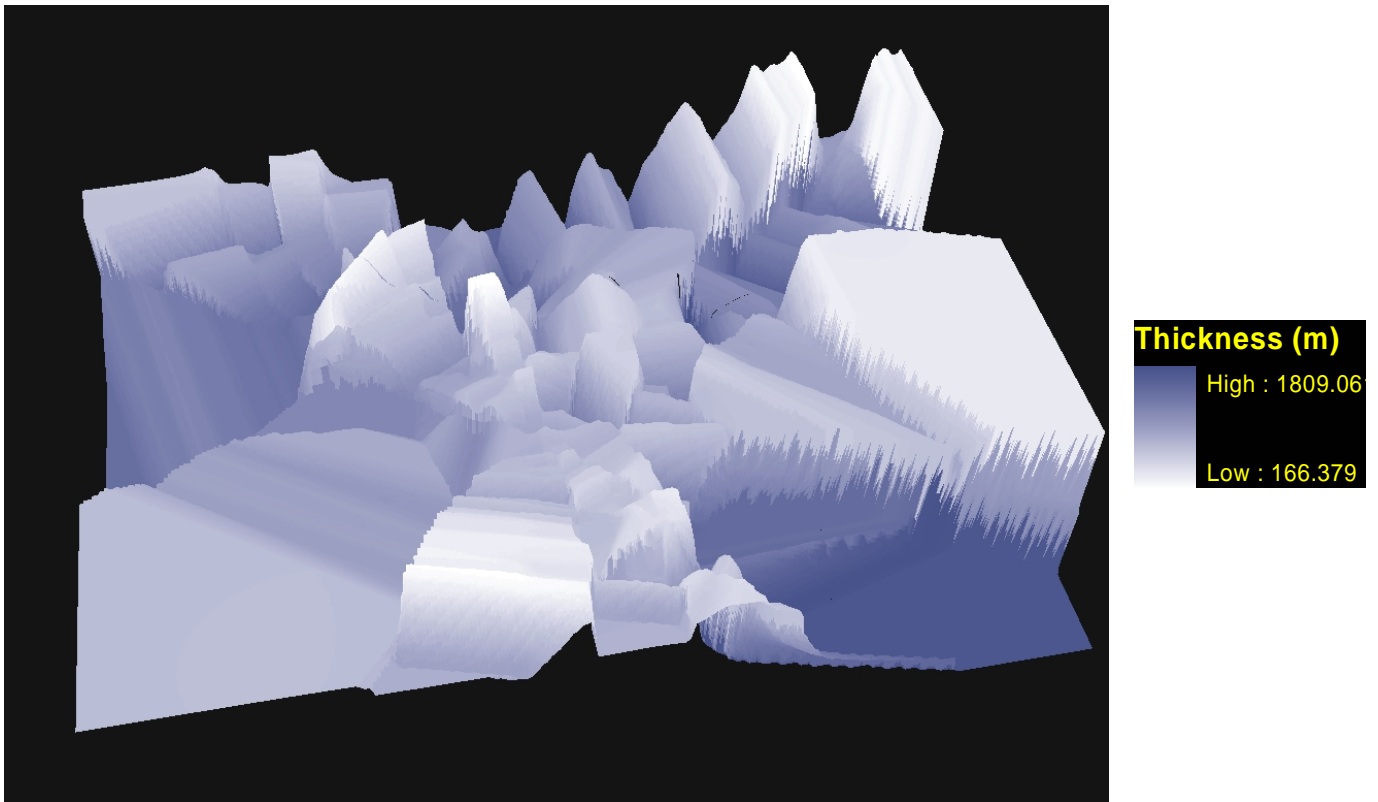


Figure 5.2 a: 3D View of the Interpolated Data over Kangerlussuaq

The bed topography at the center of the image is a more accurate prediction than the edges because of the heavy concentration of the data points in the region.

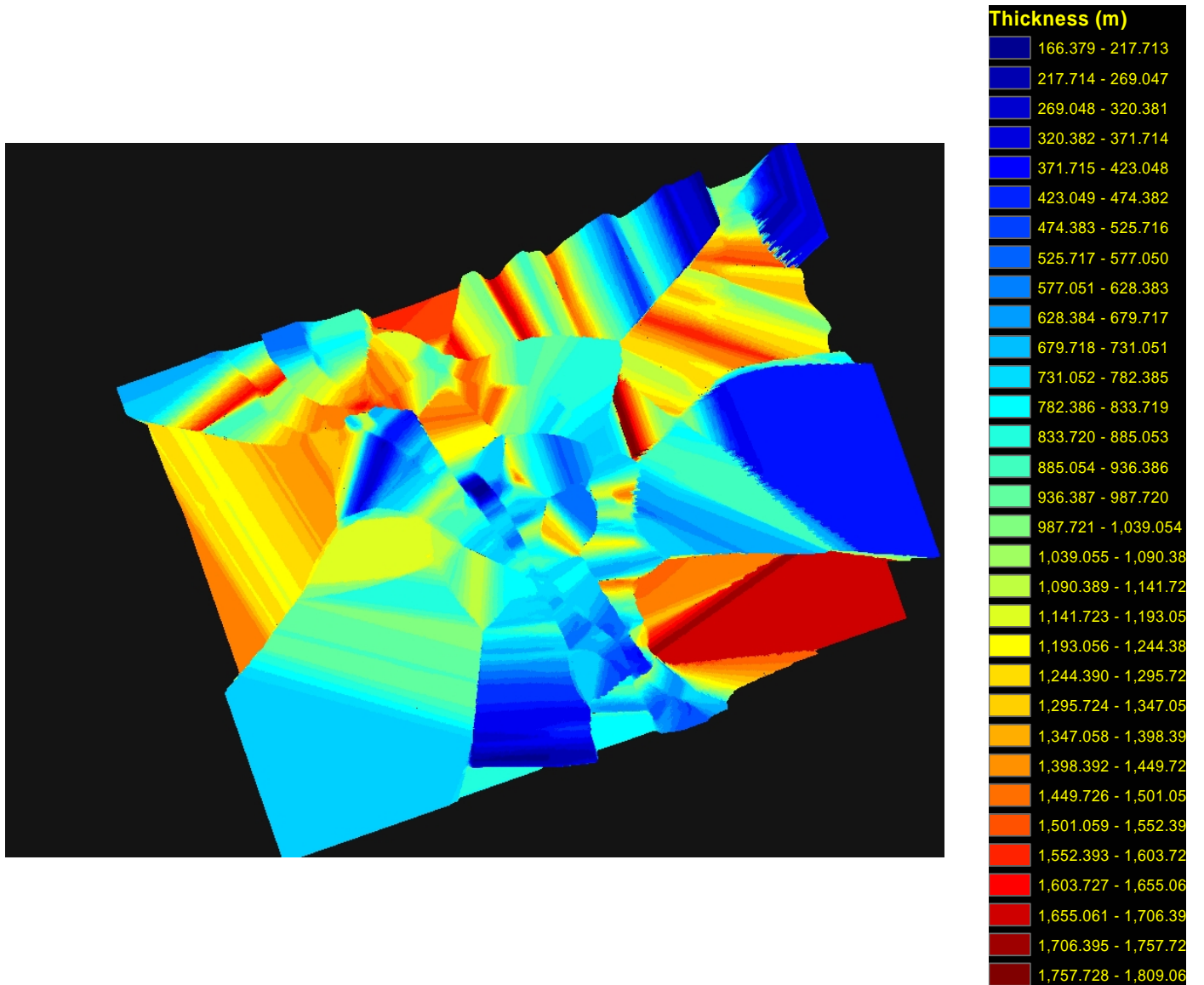


Figure 5.2 b: 3D View of the Interpolated Data over Kangerlussuaq on a Wider Color Spectrum

## 5.2 Jakobshavn Isbrae

Jakobshavn Isbrae (69.2°N 49.8°W) is the largest and the fastest moving outlet glacier in the world, with a velocity of about  $7 \text{ kma}^{-1}$  near the calving front and drains about 6.5% of the Greenland Ice sheet [7].

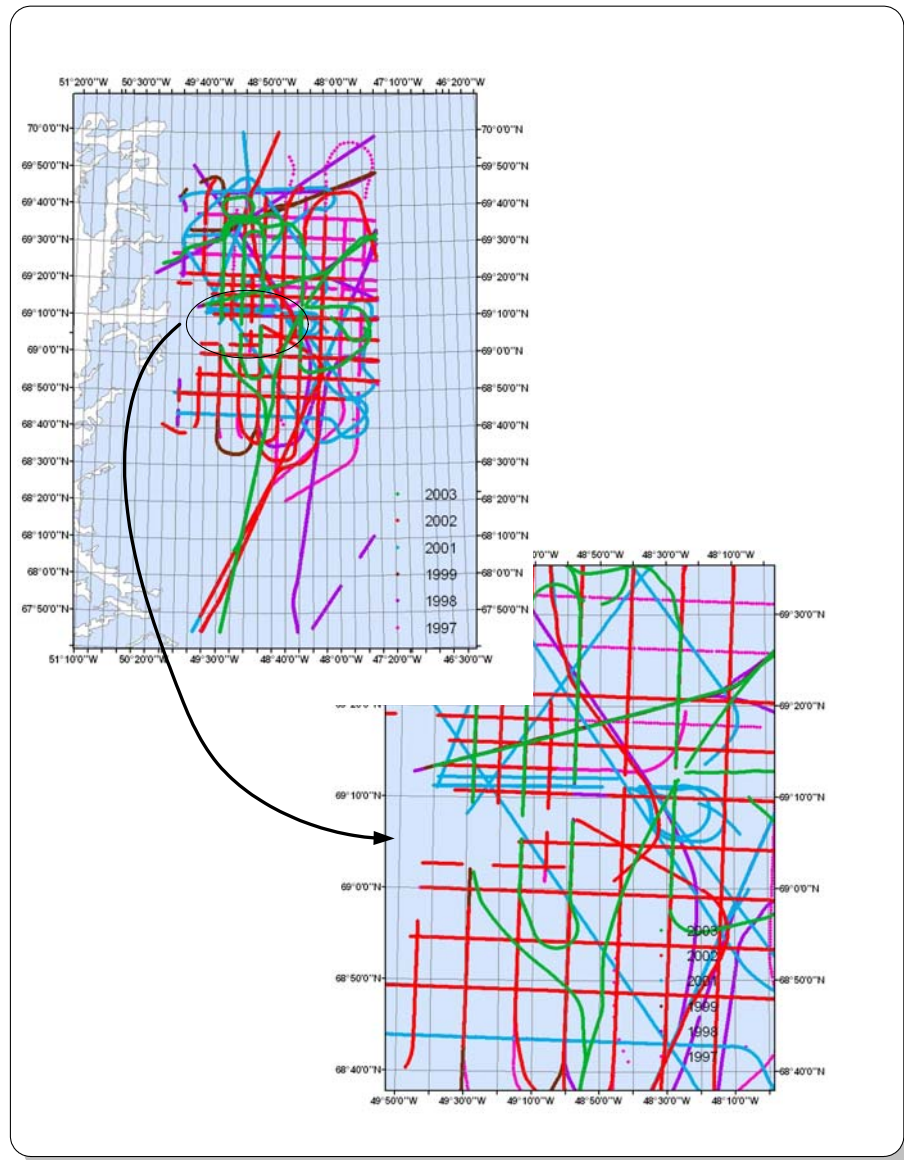


Figure 5.3 a: Flightlines over Jakobshavn Isbrae  
(Missing data across the Channel is shown)

Extensive measurements have been made in this region and the flightlines of measurements over the past six years are shown in Figure (5.3 a). Flightlines on an ASTER image along with the thickness profiles of some flight paths across the channel are shown in Figure (5.3 b). A three-dimensional map of the bed topography is generated using the thickness data from these measurements. Knowledge of the ice thickness and the bed topography helps to understand the flow mechanism of the glacier.

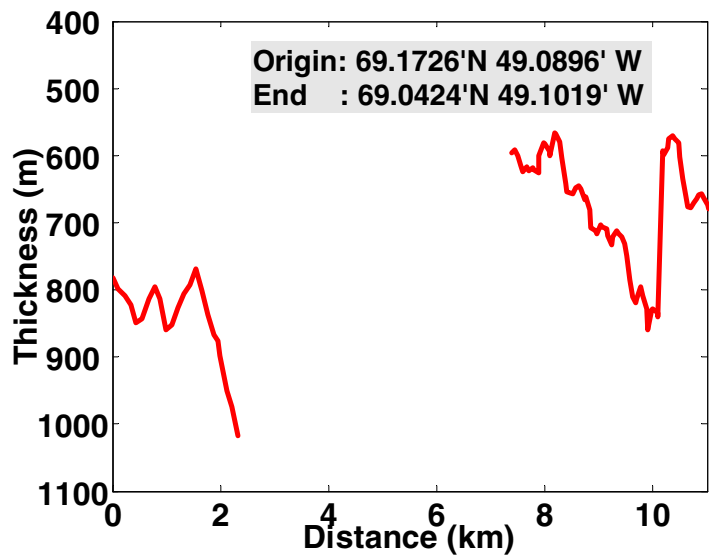
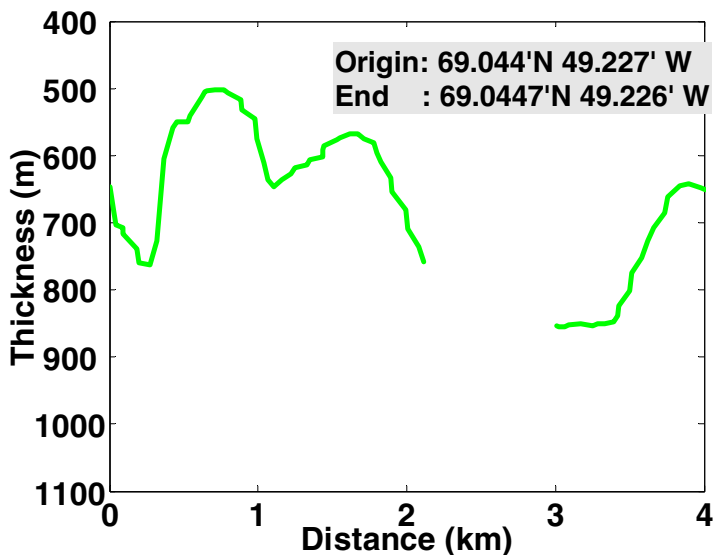
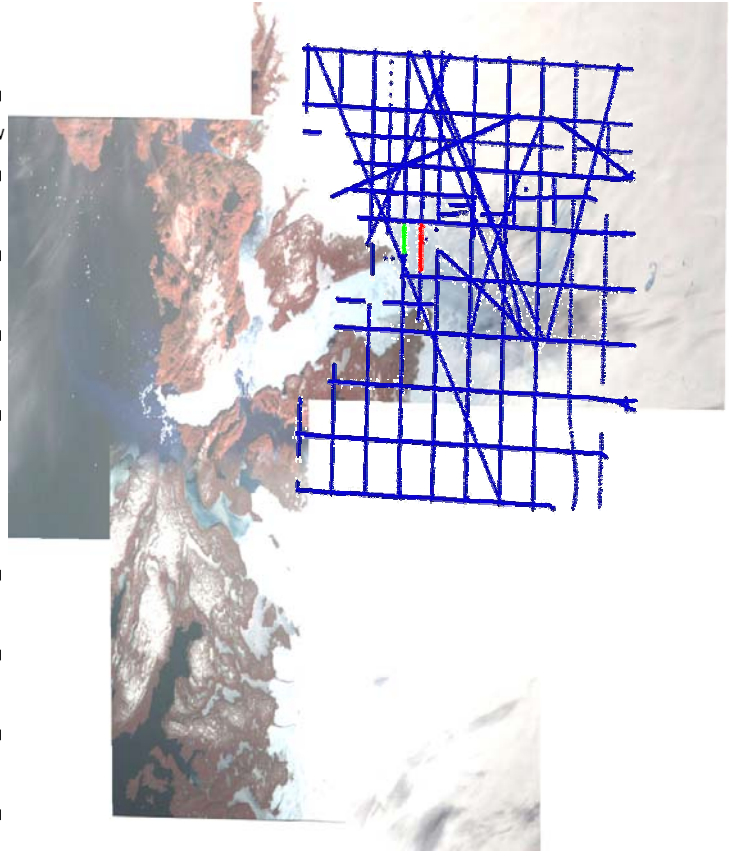
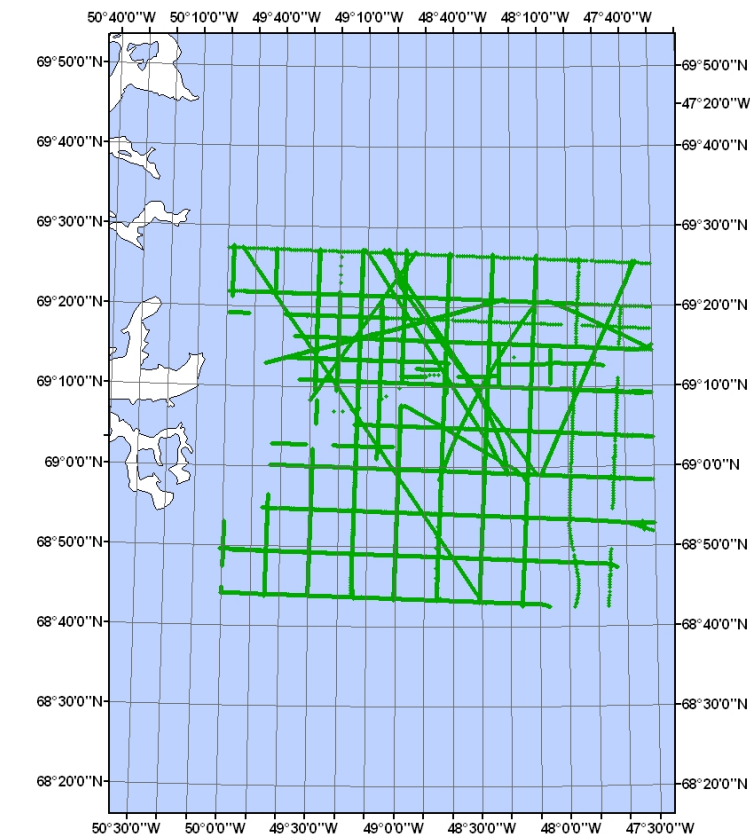


Figure (5.3 b) Jakobshavn Flightlines on a High Resolution Image of the Glacier and thickness profiles of some flight paths across the channel

## 5.2.1 Description of the Jakobshavn Dataset

Figure (5.4) shows the dataset over Jakobshavn that was used in generating the raster thickness data. The overlapping data and data collected along the flight turns were filtered out before the interpolation. As seen in the upper part of the figure, the data set is comprised of four categories of data and they are described in this section.

### 5.2.1.1 Measured Data

The data collected by radar depth sounder systems are shown in red in Figure (5.4). The flightlines are mostly in the form of grids with the along track and across track spacing of the grid being 1 km. The depth sounder systems have not been successful in identifying the basal return along a major portion of the ice stream from about  $69^{\circ}15''$  N  $48^{\circ}50''$  W to about  $69^{\circ}50''$  N  $49^{\circ}25''$  W (see Figure 5.3 a). This is due to strong surface scatter masking the return from the bedrock. The few crossing points in the region, collected in the previous years were reanalyzed and erroneous data were eliminated. Missing data in the channel were filled with seismic data [14], synthetic data and some “dummy” data to model the channel. These are described in the following sections.

### 5.2.1.2 Seismic Data

Seismic reflection methods [14] were used to determine the depth of bedrock in the channel. The centerline ice thickness was observed to be about 2500 m, which is

2.5 times greater than that of the surrounding ice sheet. Thickness data from these seismic reflections at four different regions across the channel were integrated with the data from radar  sounding. Seismic data are shown in green in the upper half of Figure (5.4).

### **5.2.1.3 Synthetic Data**

Figure (5.5) shows an echogram from the data across the channel and its thickness plot. It can be observed from the echogram that the return from the bed is prominent until about the 500<sup>th</sup> record, when there is a steep increase in the thickness from about 1000 m to about 2.05 km, and the bed return reappears at around the 575<sup>th</sup> record. This appears as a discontinuity in the flightpath of Figure (5.3). Data is synthesized by interpolating the bed echo along the flightpath with the interpolation conforming to the knowledge of the depth of the channel as observed by the seismic reflections. Synthetic data are shown in yellow in the upper half of Figure (5.4).

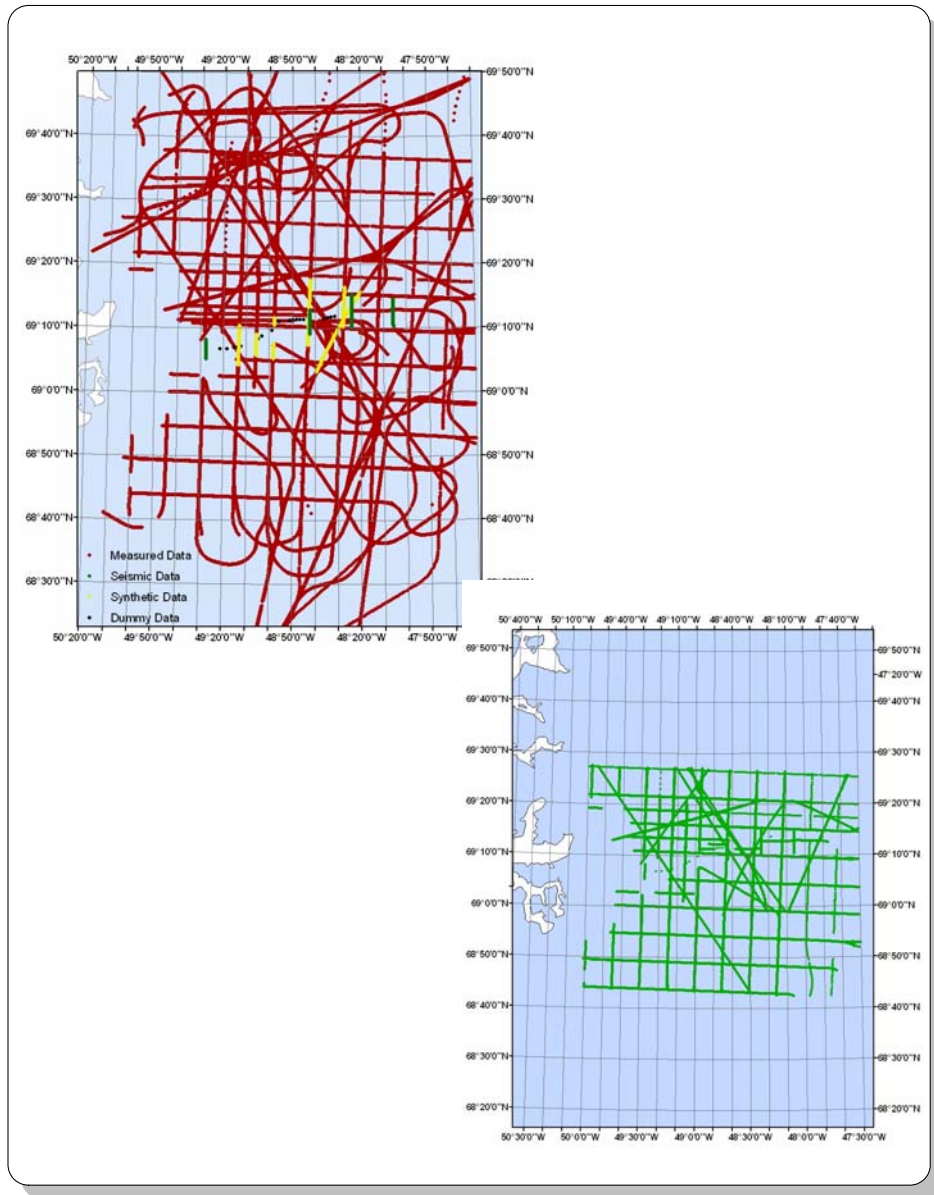


Figure 5.4: Data Description and Data Filtering over Jakobshavn

#### **5.2.1.4 “Dummy” Data Points**

Some false points are added to the previous three categories of data at places where there are no data across the channel. These “dummy” data points are based on knowledge of thickness along the channel from seismic reflection. These data points are added to help in interpolating the channel topography and are kept to a minimum. These points are shown as black dots in the upper half of Figure (5.4).

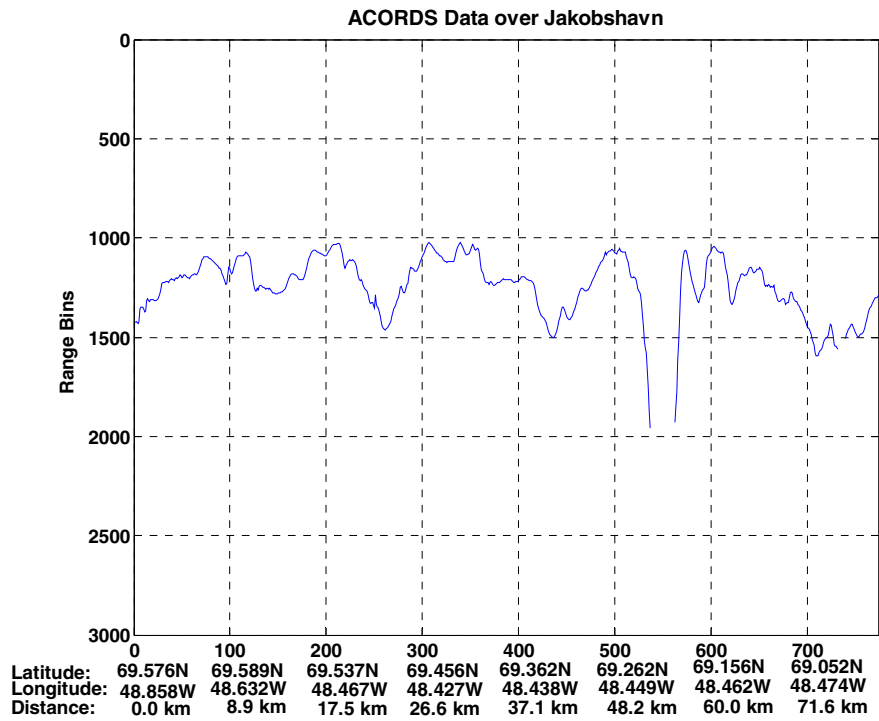
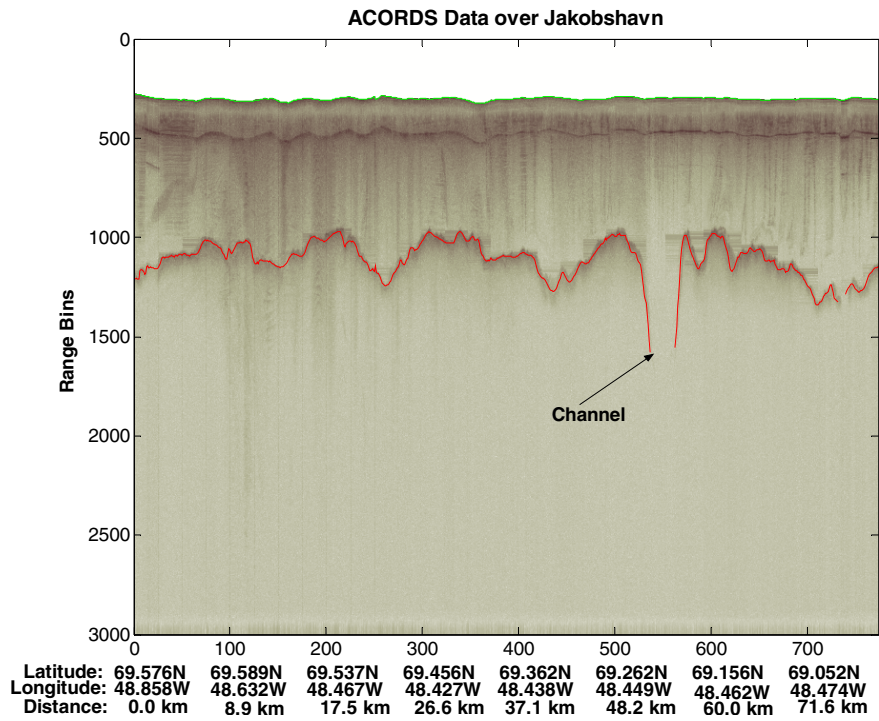


Figure 5.5: Echogram Illustrating the Channel in Jakobshavn and the Thickness Profile Across the Channel

**Interpolation to Raster Thickness Data**

All the above categories of data are integrated into a single data set and interpolated to a raster by kriging. Similar to interpolating the data set of Kangerlussuaq, spatial correlation among the values is used to model the interpolation method. The interpolation method is then validated and implemented on the data set.

#### **5.2.2.1 Design**

The Semivariogram plot of Jakobshavn was fit with an exponential curve and the sill was found to be 177.44 km. The model is anisotropic and accounts for the nugget effect, measurement errors and overlapping data points.

#### **5.2.2.2 Validation**

Both exponential fit and spherical fit for the semivariogram were equally unbiased with almost similar values of mean standard error of around 0.001. But the exponential model is a more precise model because the rms prediction error (27.64) is closer to the average standard error (43.21). For the spherical model, the rms prediction error and the average standard error were 45.27 and 132.5 respectively. As discussed earlier, the smaller the difference between the rms value to the average standard error, the higher the level of confidence in the prediction.

Jakobshavn channel is also modeled by an exponential fit for the Semivariogram, which performs better than a spherical fit.

### 5.2.2.3 Implementation

Values of nugget, sill and range are obtained from the validated model to create the weight matrix and predict the unknown values in the raster.  data is interpolated using twelve neighboring samples to a raster of cell size 200 m. When interpolating only the data from the channel, the output cell size is specified to be 50 m because of the relatively smaller number of input points for the interpolating the channel.

### 5.2.2.4 Results

The bed terrain map of Jakobshavn glacier is shown in Figure (5.6) along with the map of the channel alone. In interpolating the channel, the interpolation model was designed with the points that were within the close neighborhood of the channel. This is a more valid model for the channel with mean standard error of 0.0005538 and rms prediction error of almost unity (0.8819). So the channel interpolated separately depicts the true terrain more closely than the overall model.

As shown in Figure (5.6), the trough-like formation near the center has a thickness of about 2500 m along the centerline and becomes shallow and wider near the calving front.

The bed topography is shown in Figure (5.7 a) and Figure (5.7 b) on a more classified color spectrum.

Since there are no data near the calving front from either seismic reflections or depth soundings, the interpolation in a 15 km-wide channel (near 69.18N 49.56W) leading to the calving front is unreliable. This region is circled in red in the following images.

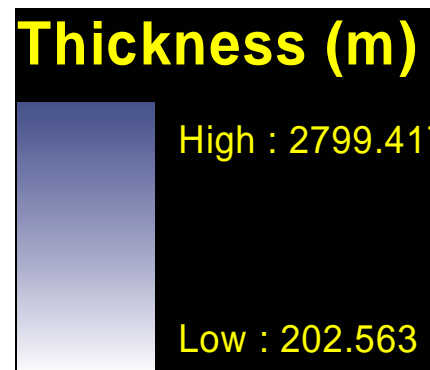
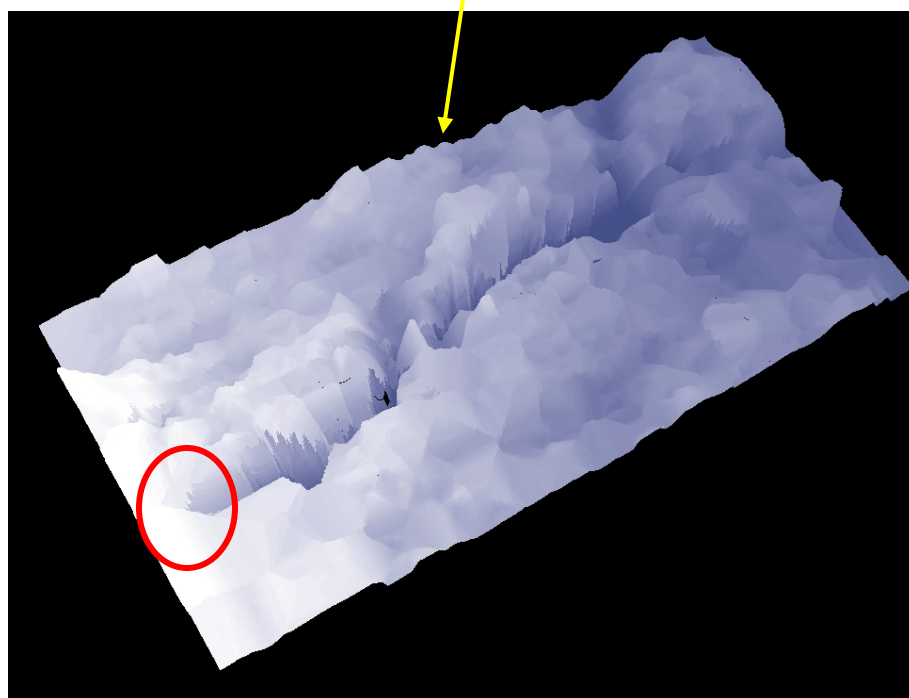
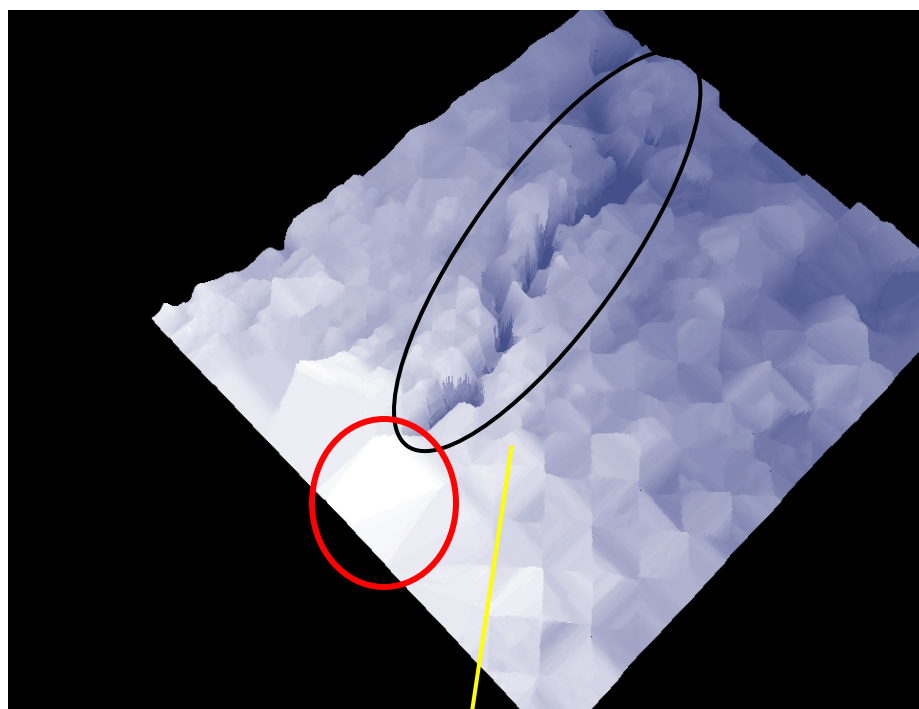


Figure 5.6: Interpolated Bed Topography of Jakobshavn (above); View of the Interpolated Channel (below)

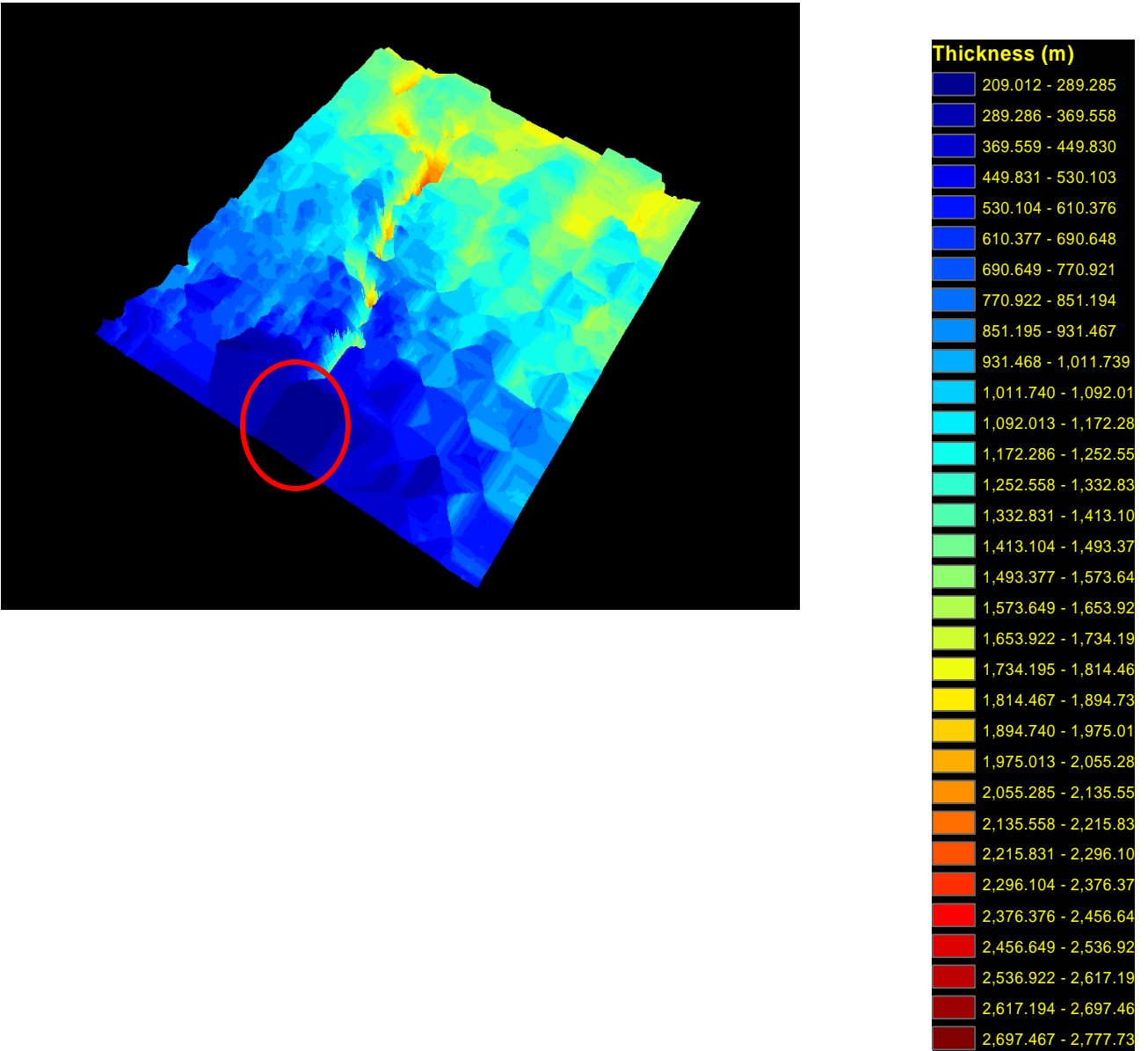


Figure 5.7 a: 3D View of the Interpolated Data over Jakobshavn on a Wider Color Spectrum

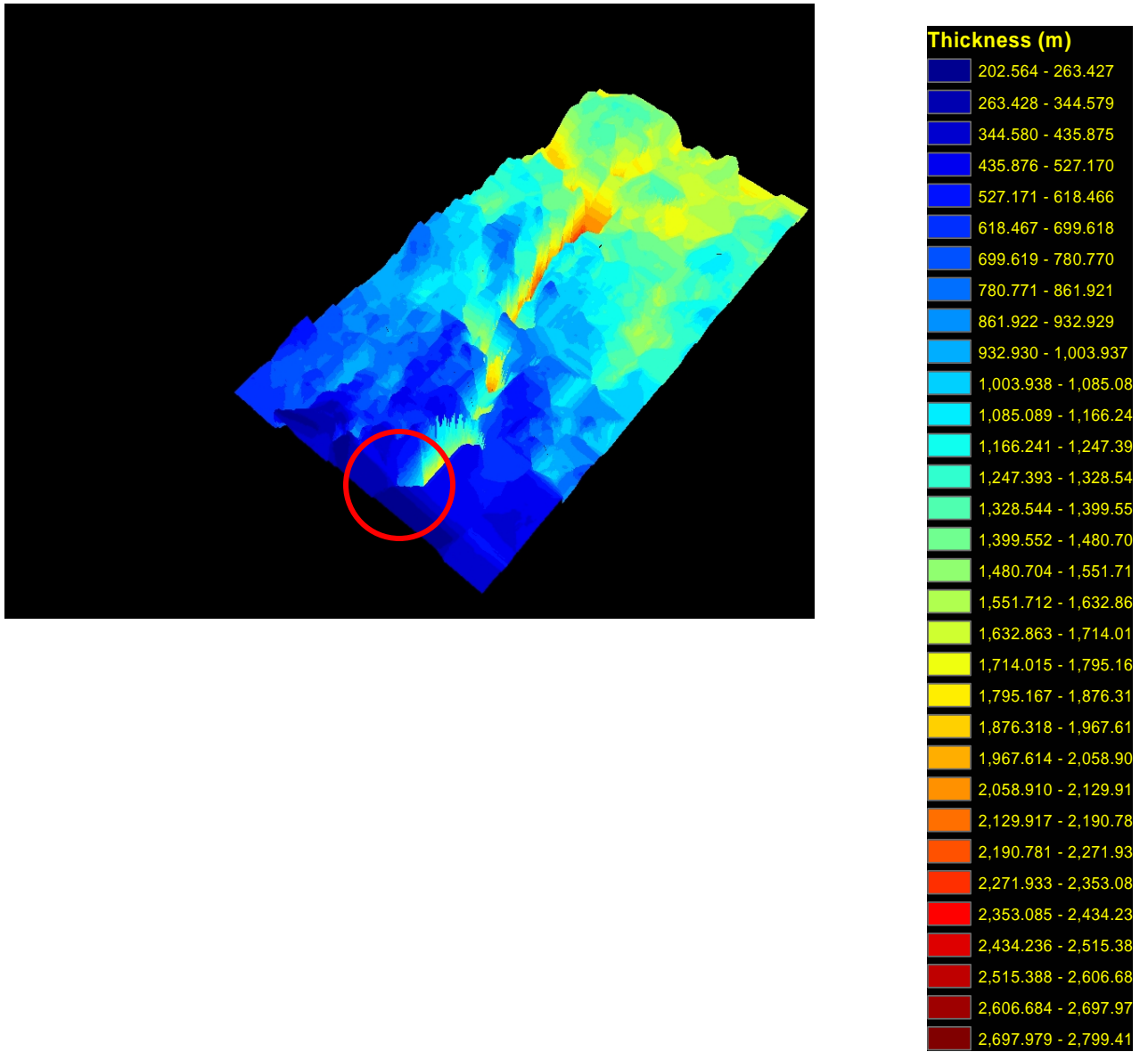


Figure 5.7 b: 3D View of the Interpolated Data over Jakobshavn Channel on a Wider Color Spectrum

### 5.3 Petermann Glacier

Petermann Glacier (80.6°N and 60°W) is the largest and the most influential outlet glacier in Northern Greenland [14]. Data from this region have been interpolated into a raster, and a 3D image of the floating ice tongue has been generated.

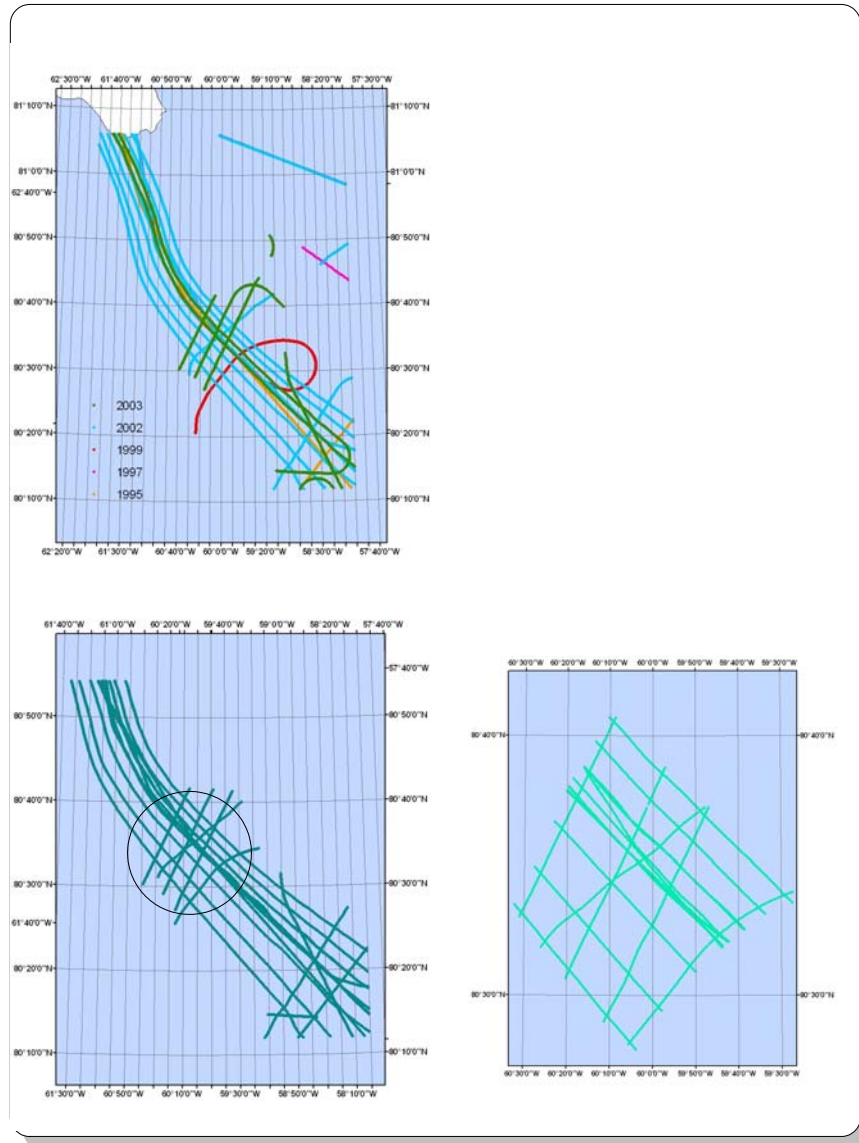


Figure 5.8 a: Flightlines over Petermann Glacier

The flightlines along which depth sounder measurements were made over Petermann Glacier from 1995 to 2003 are shown in Figure (5.8 a). The radar data collected by ACORDS in 2003 over this region have been processed and integrated with the data from the previous years. The distance between the flightlines along the channel is about 3.5 km at the bottom of the channel. The spacing between the flightlines is narrower up the channel, and the separation between them is about 1.8 km near the calving front. The crossovers at the center of the Petermann channel are spaced at about 5 km apart. Crossover data were used to assess the accuracy of the data sets. Any erroneous data were corrected using crossover analysis. As seen in the bottom half of Figure (5.8 a), data along the flight turns were filtered out to avoid error due to aircraft banking. Figure (5.8 b) shows the flightlines on an ASTER image along with the thickness profiles of the crossovers.

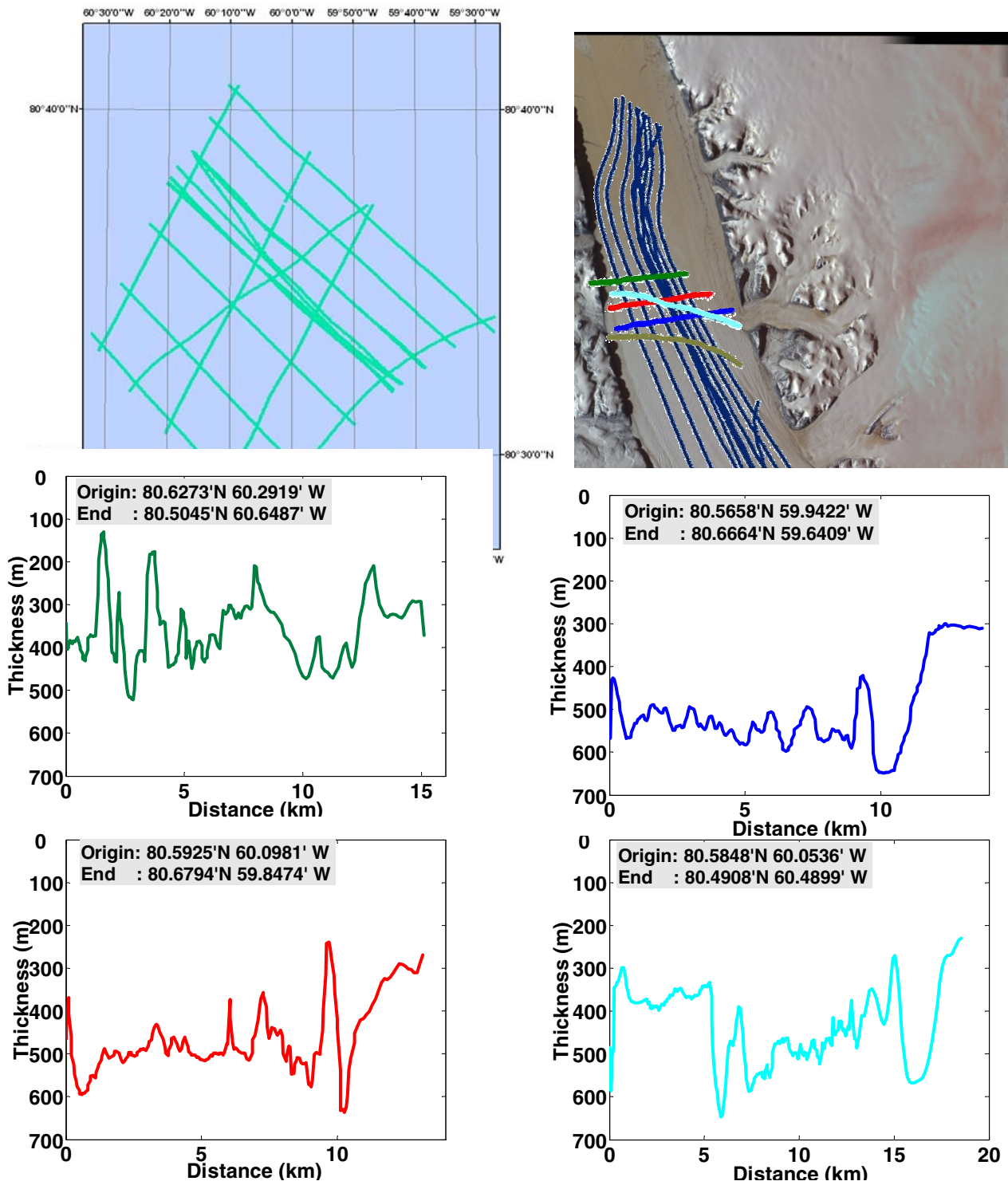


Figure 5.8 b: Petermann Flightlines on a High Resolution Image of the Glacier and Thickness Profiles of crossovers

### **5.3.1 Interpolation to Raster Thickness Data**

The filtered data set is interpolated to a raster by kriging. Similar to the previous two cases, the spatial correlation between the thickness values was first quantified and used to design an interpolation model. The model is then validated and implemented.

#### **5.3.1.1 Design**

The Semivariogram plot of the Petermann data set was fit with an exponential curve and the sill was found to be 145 km. Hence the points that were separated by more than 145 km had no spatial relationship. The designed model accounts for anisotropy, nugget effect and measurement errors.

#### **5.3.1.2 Validation**

Both exponential fit and spherical fit for the Semivariogram of the Petermann data set had similar bias, but the spherical model was a more precise model because the prediction using a spherical fit assessed the variability in the prediction more accurately. However, the exponential model predicted better when interpolating the central region of the channel with crossovers. In this case the exponential fit gave a mean standardized error of 0.002206 as against 0.004426 by the spherical fit.

### **5.3.1.3 Implementation**

The design parameters obtained above were used to generate the raster for the data set. The output cell size was chosen as 100 m, and for the raster in the region of the crossovers, the cell size was chosen as 50 m, because of the relatively smaller area, a smaller cell size gives finer resolution.

### **5.3.1.4 Results**

The bed terrain map of Petermann glacier is shown in Figure (5.9) with the crossover region at the center of the channel. Figures (5.10 a) and (5.10 b) illustrate the same figure on a wider color spectrum.

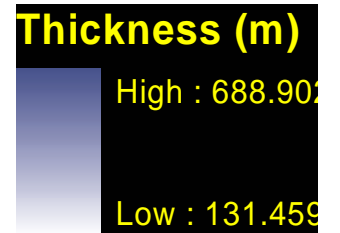
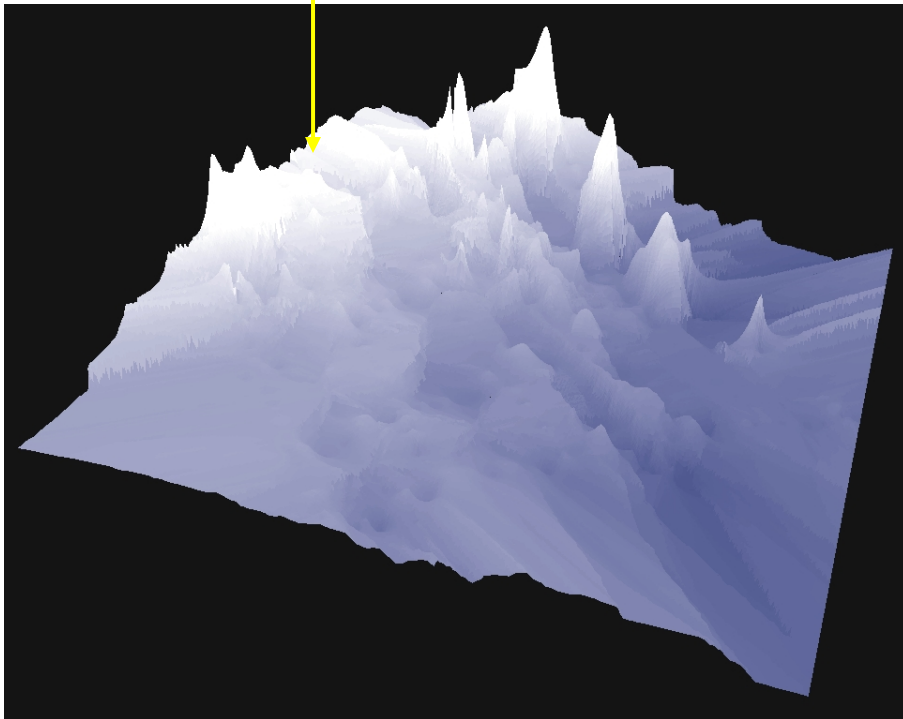
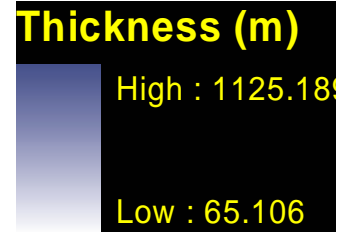
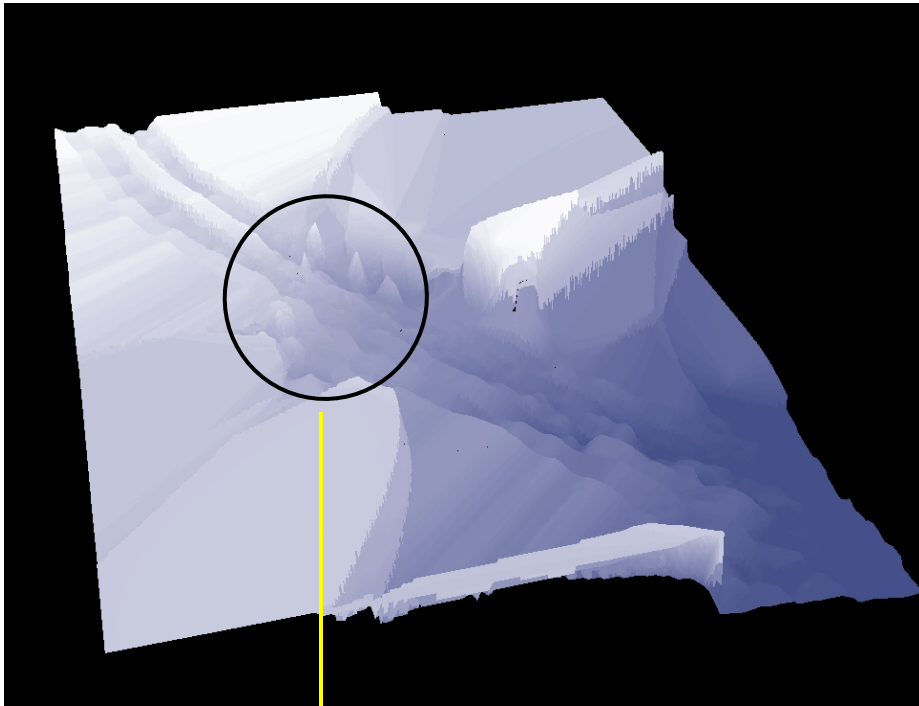


Figure 5.9: Interpolated Bed Topography of Petermann (above); Crossover Region (below)

As it can be observed, the thickness of the ice sheet decreases rapidly as we move up the channel, near the grounding line. This is more evident from the radar echogram shown in Figure (5.11).

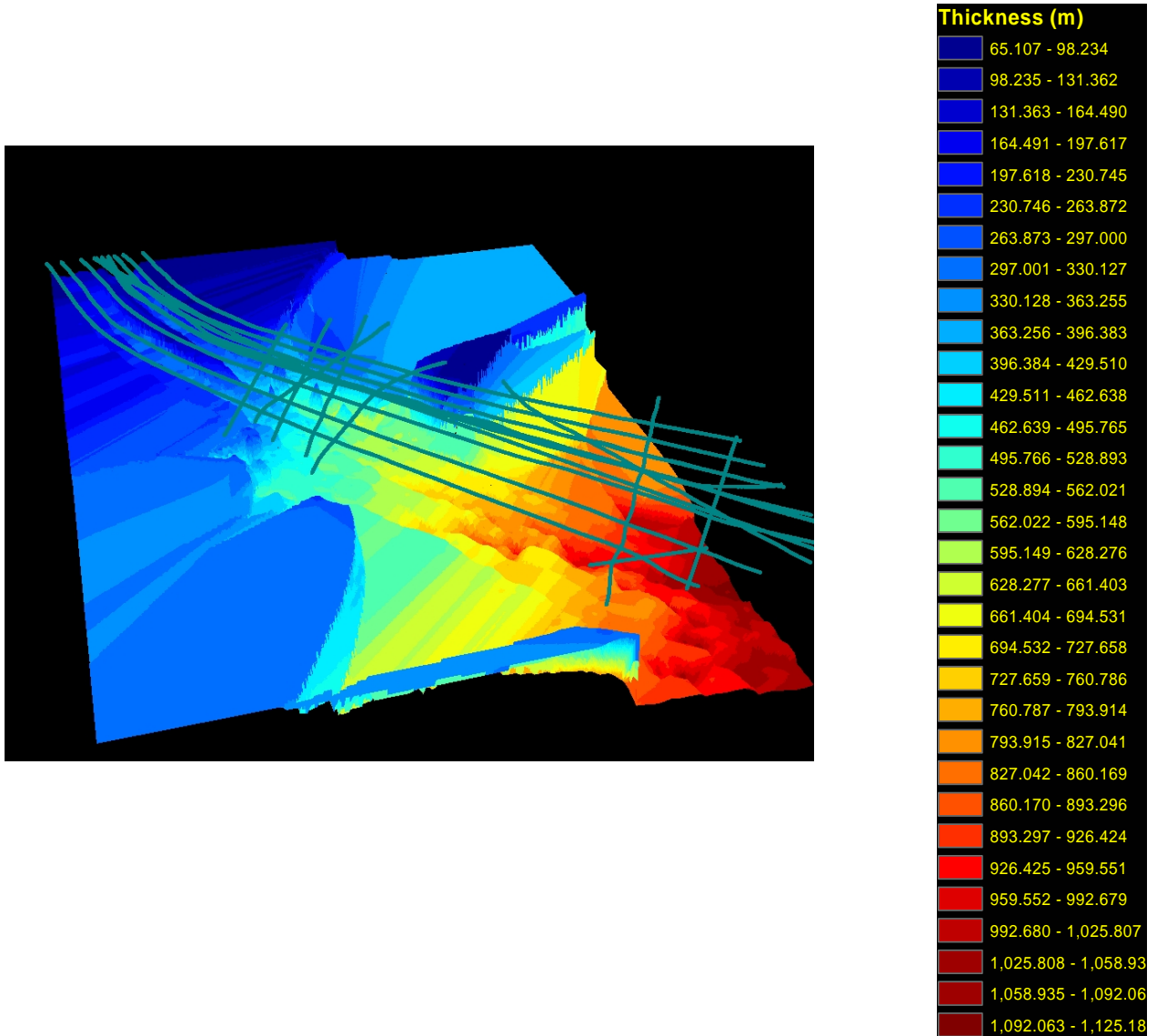


Figure 5.10 a: 3D View of the Interpolated Data over Petermann on a Wider Color Spectrum

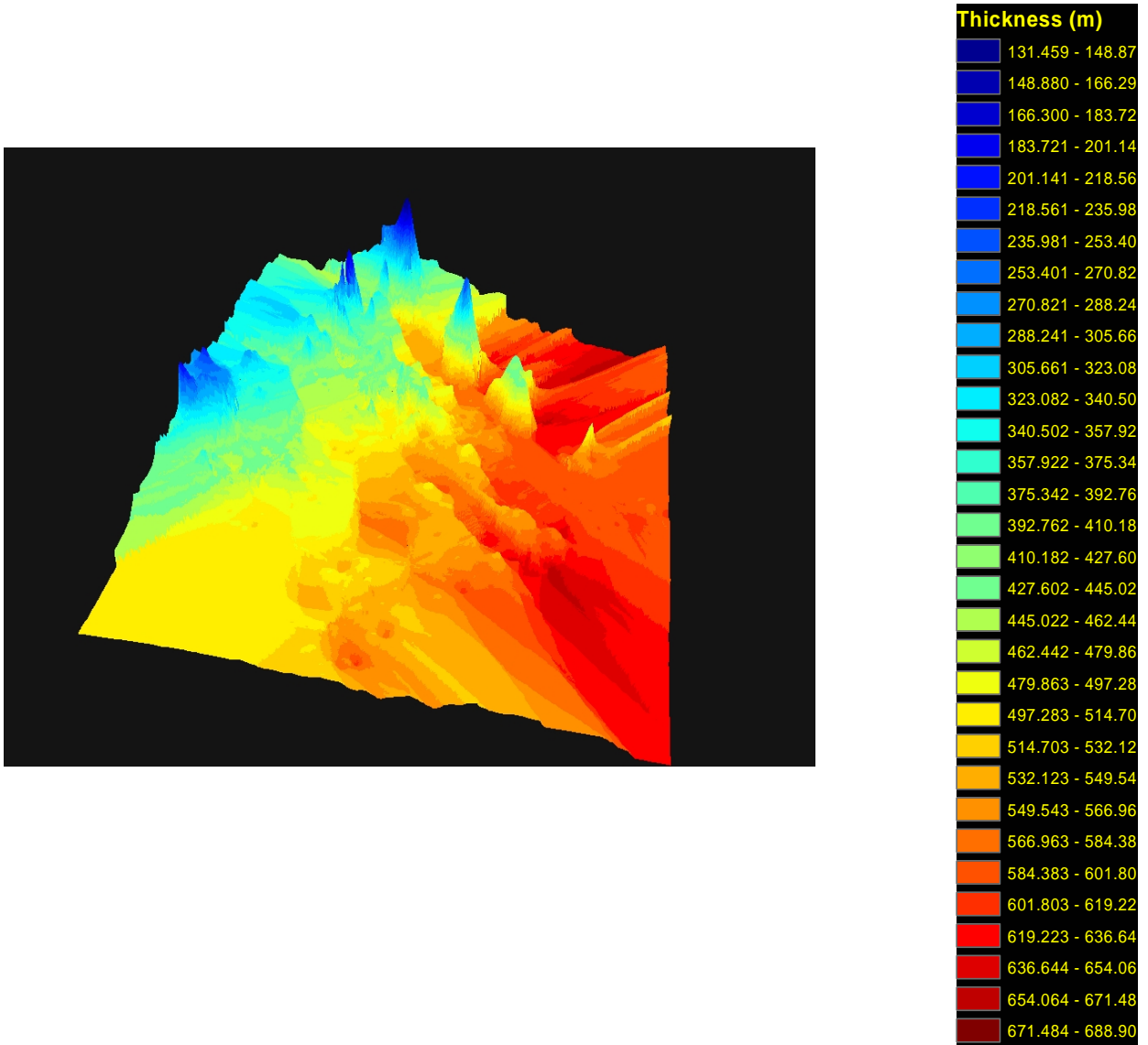


Figure 5.10 b: 3D View of the Interpolated Data over Crossover Region on a Wider Color Spectrum

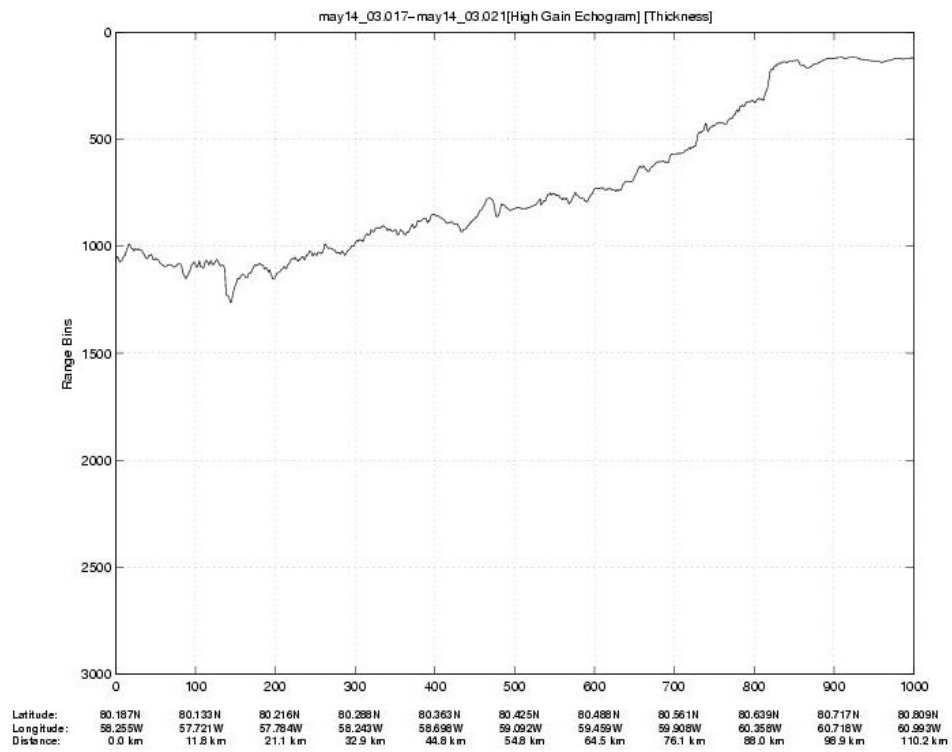
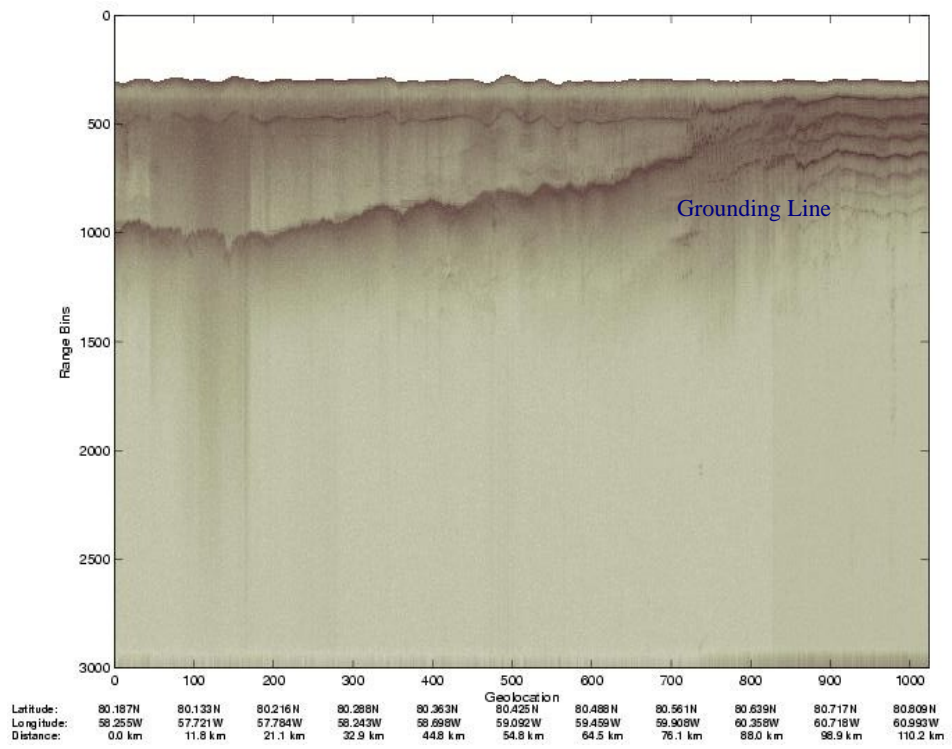


Figure 5.11: Echogram and Thickness Plot of Petermann Up the Channel Towards the Grounding Line

As seen in the image of Figure (5.9) and confirmed by the thickness plot of Figure (5.11), there is a rapid decrease in the thickness from about 450 m to 60 m near the calving front within a distance of 30 km.

The ridge-like artifact found along the center line of the channel from near its center up the calving front has been accounted for by [10] as medial moraine, which is a ridge of glacial debris formed when two valley glaciers join to form a single ice stream.

As an addition, zero ice thickness areas have been included over nunataks (small rocky areas) so that ice thickness drops to zero along these areas. This image is shown in the appendix.

## **6 Conclusion And Future Work**

### **6.1 Conclusion**

Airborne measurements were made for the first time over Pine Island and Thwaites glaciers in Antarctica. The radar signal returns from glacial ice collected over these regions by the Improved Coherent Antarctic and Arctic Radar Depth Sounder (ICARDS) have been processed to determine the thickness of glacial ice. Ice thickness was measured over 99% of the PIG and TG flightlines.

The radar signal returns from glacial ice collected over Greenland by the Advanced COherent Radar Depth Sounder (ACORDS) in the summer of 2003 have been processed for high-resolution thickness. Various signal-processing operations have been performed to improve the signal-to-noise ratio and reduce coherent noise in the data. Multipath phenomenon, involving radar returns from the ice surface and the chassis of the aircraft, has been eliminated in the regions where these multiple echoes were impairing accurate interpretation of radar returns from the ice/bed interface.

Ice thickness data from 2003 have been included with the data from the previous six years to produce a three-dimensional image of the bedrock. Understanding the

dynamics of glacial flow is critical because the outlet glaciers drain a major portion of the Greenland ice sheet. The flow pattern of glaciers over the ice sheet is controlled by the bed topography. Hence, the three-dimensional image of the ice thickness is a step toward obtaining bed topography. These depth sounder systems help scientists better understand the characteristics of glacial flow and ice sheet behavior.

A Digital Ice Thickness Model for the bed has been generated from the interpolated raster for the three major outlet glaciers of Jakobshavns Isbrae, Petermann and Kangerlussuaq.

## **6.2 Pointers to Future Work**

Gridded flightlines over Jakobshavn provided a large number of measured data points to interpolate from and this resulted in an accurate prediction of thickness for the unknown areas. Flightlines over Kangerlussuaq have to be in the form of grid to be able to model the bed topography and understand the dynamics of the glacier. These grid lines can be spaced about 1 km apart along and across the track. Flightline crossovers can be used in analyzing the existing data for errors.

More data can be collected across the channel in Petermann, especially nearing the calving front. This will help in accounting for the artifacts in the floating tongue of the glacier.

An elevation grid for the surface can be developed and combined with bed digital ice thickness grid developed here to produce a bed elevation for the outlet glaciers.

## References

---

[1] C.Allen, B.Wohletz, and S.Gogineni, “Radar Sounding of Glaciers in Greenland,” *IGARSS 96*, May 1996, Lincoln, NE.

[2] Dr. David Whitehouse, “Greenland Ice cap under threat,” *BBC News*, April 7, 2004.

[3] Richard S.Williams,Jr., “Glaciers and Glacier Landforms,” *Geomorphology from Space*.

[4] S.Gogineni, T.Chuah, C.Allen, K.Jezek, and R.K.Moore, “An Improved Coherent Radar Depth Sounder,” *Journal of Glaciology*, vol. 44, no. 148, pp. 659 – 669, 1998.

[5] T.S.Chuah, “Design and Development of a Coherent Radar Depth Sounder for Measurement of Greenland Ice Sheet Thickness,” Ph.D Dissertation, Electrical Engineering and Computer Science, The University of Kansas, Lawrence, Kansas, 1996

[6] Saikiran P.V. Namburi, “Design and Development of an Advanced Coherent Radar Depth Sounder,” M.S. Thesis, Electrical Engineering and Computer Science, The University of Kansas, Lawrence, Kansas, 2003

[7] C.Allen, S.Gogineni, B.Wohletz, K.Jezek and T.Chuah, “Airborne Radio Echo Sounding of Outlet Glaciers in Greenland,” *International Journal of Remote Sensing*, vol. 18, no. 14, pp. 3103 – 3107, 1997.

[8] Torry Lee Akins, “Design and Development of an Improved Data Acquisition System for the Coherent Radar Depth Sounder,” M.S. Thesis, Electrical Engineering and Computer Science, The University of Kansas, Lawrence, Kansas, 1998.

[9] M. Skolnik, *Introduction to Radar Systems*, McGraw Hill, Third Edition, New York, 2001.

[10] W.K. Saunders, “CW and FM Radar,” in *Radar Handbook*, edited by M.Skolnik, 14.1 – 13.45, 1990.

[11] Land Processes DAAC (LP DAAC) User Services, U.S. Geological Survey, EROS Data Center

[12] M. Luthi, M. Funck, A. Iken, S.Gogineni, M. Truffer, “Mechanisms of Fast Flow in Jakobshavn Isbrae, West Greenland: Part III. Measurements of Ice Deformation,

Temperature and Cross-borehole Conductivity in Boreholes to the Bedrock,” *Journal of Glaciology*, vol. 28, no. 162, pp. 369 – 385, 2002

[13] T. Clarke and K. Echelmeyer, “Seismic–Reflection Evidence for a Deep Subglacial Trough Beneath Jakobshavns Isbrae, West Greenland,” *Journal of Glaciology*, vol. 43, no. 141, pp. 219 – 232, 1996.

[14] K. Steffen, R.D. Huff, N. Cullen, E. Rignot, C. Stewart and A. Jenkins, “Channel-Like Bottom Features and High Bottom Melt Rates of Petermann Gletscher’s Floating Tongue in Northwestern Greenland,” American Geophysical Union fall meeting, vol. 84, no.46, 2003.

[15] K. Steffen, Cooperative Institute for Research in Environmental Science, University of Colorado, Boulder, CO.

## Appendix

---

### Petermann Glacier

The figure below shows the ice thickness map of Petermann after including zero ice thickness over the areas of rock.

